International Journal of Engineering Research in Africa
ISSN: 1663-4144, Vol. 53, pp 123-156

Submitted: 2020-05-21
Revised: 2020-11-01
Accepted: 2020-12-09
Online: 2021-03-04

A Modified Corner Detector for SAR Images Registration

Abdelhameed S. Eltanany[1,a], A. S. Amein[2,b*] and M. S. Elwan[3,c]

[1]Electrical Engineering Department, Military Technical College (MTC), Egypt

[2] Faculty of Information Systems and Computer Science, October 6 University, Egypt

[3]Egyptian Academy of Engineering and Advanced Technology (EAEAT), Egypt

[a]abdotanany@hotmail.com, [b]ahmed.saleh.csis@o6u.edu.eg, [c]msafy@eaeat.edu.eg

Keywords: Feature Detection, Harris Corner Detector, Image Registration, Phase Congruency, Random Sample Consensus (RANSAC).

Abstract. As a first step for image processing operations, detection of corners is a vital procedure where it can be applied for many applications as feature matching, image registration, image mosaicking, image fusion, and change detection. Image registration can be defined as process of getting the misalignment of pixel's position between two or more images. In this paper, a modified corner detector named Synthetic Aperture Radar- Phase Congruency Harris (SAR-PCH) based on a combination between both phase congruency, named later PC, and Harris corner detector is proposed where PC image can supply fundamental and significative features although the complex changes of intensities. Also, the proposed approach overcomes the Harris limitation concerning the noise since the Harris is more sensitive to the noise. The performance was similitude with Shi-Tomasi, FAST, and Harris corner detectors where experiments are conducted first with simulated images and second with real ones. Mean square error (MSE) and peak signal-to-noise ratio (PSNR) are used for the simile. Experimental results, carried out in a standard computer, verify its effectiveness where it utilizes the privileges of image constitutional depicting, allowing extraction of the most powerful key points since it preserves robustness of co-registration process using image frequency properties which are not variant to illumination. Reasonable results compared to the state of art method as Shi-Tomasi, FAST, and Harris algorithms were achieved on the expense of high computational processing time that can be recovered using hardware having high capabilities.

1. Introduction

Performing image registration process enables finding the correspondence among the input images by estimating necessary transformation matrix to adjust positions of selected points in sensed image with its correspondence in matched one. Feature detection is an essential step for images interpretation to be applicable in various applications as image registration. Image registration has two main approaches; first is called area-based matching method (ABM) where feature existence is ensured rather than detection. The other approach is called feature-based matching method (FBM) where the process of detection plays a vital step. Generally, each approach has advantages differentiating it than the other and at same time; it has its disadvantages which could be recurred using the other approach [1-5]. Features may be global or local where the global ones represent the image as a whole and the local ones represent specific patches in the image. Feature may be corners, edges, texture, color, or blobs [6-9]. Global features have a limitation and can be recovered using certain techniques as segmentation [8-10].

Based on the properties of structure stability and informativeness; the usage of local features is preferred since the process of distinguishing a group of noteworthy points can be achieved where the points have specific properties [6-11]. Multiple techniques for feature detection had been developed taking into consideration the required application where the behavior of their performance is related to parameters of their design. So; there is no a common ideal algorithm for registration process since each algorithm is based on a special request. Any detector should have a certain characteristic and also the good feature has [2, 8-11].

Since many definitions for the corner are illustrated where the detection accuracy is affected by the data imperfections as geometric and radiometric distortions, so the target of the detection process is to collapse the similar features in spite of these imperfections. In case of the stability structure of the information shape (invariant), issues relating to translation; rotation; and scaling can be treated easily. Detection process is more difficult to be handled concerning projective and affine problems [8, 9, 12]. So; the feature detection methodology should be not sensitive to the general geometric and radiometric distortions. There are many techniques had been proposed [1-3, 8-12]. Finally, categorization of feature detectors can be achieved according to operating principle and operating scale [4, 8, 10].

Generally, registration's target is having the right transformation matrix to represent points in one image to its congruent in the other depending mainly on feature detection to align the images (two or more). Values of matrix's parameters should satisfy the in-demand estimations of the similarity metrices leading to getting the required value of nearness or stage of suitability between images and this can be achieved by increasing the mutual information between the inputs.

It is very important to know that one algorithm for registration couldn't be utilized as a generic approach for all images since each algorithm is designed to perform a specific mission and may fail to achieve another. Registration algorithms consist of three phases 1) detection of key points (features) related to input images, 2) possessing the required transformation model that link these key points, 3) owing the cost function for the similarity metric measurements providing the suitability grad among the inputs. Many detector approaches based on feature detection use the behavior of the gray information to extract key points, so it is easily influenced by speckle noise which is variations of contrast; noise; and illumination. These variations will cause the features to be unstable and imprecise localized. Latterly, some adjustments have been developed as using adaptive weighted filtering process having a high computation cost with more complexity to deal with variations leading to losing of important data [1-12].

This paper is structured as follows; the relevant works concerning this research field are presented in section two. In sections three and four, the Phase Congruency (PC) algorithm and the Harris corner detector are presented. The framework, including the proposed structure, experimental dataset, assessment criteria, outcomes, results and analysis, is discussed in section five. Finally, the conclusion is given in section six.

2. Related Work

Wenping Ma in [13] proposed a methodology that is based on a combination of both frequency domain and spatial domain where Phase Congruency (PC) approach is used beside SAR-SIFT spatial constraints. The features are detected from the corresponding PC images after being applied to SAR-SIFT descriptor. It provides a meaningful image features depending on the advantages of phase congruency algorithm. The approach was compared to the state-of-the-art approaches as SIFT and SURF where it acts as a descriptor. Zaafouri A. in [14] tries to extract the two main linear features in the satellite images, step and line features. The method is based on usage of phase congruency (PC) algorithm combined with non-linear contextual smoothing approach. In [15], Jyoti Malik and G. Sainarayanan proposed a Phase Congruency Corner Detector (PCCD) approach in order to detect and extract the features of palmprint as a corner’s form. PCCD is combined with Matching similarity measurement technique, correlation, to detect and extract the palmprint features, then; stored and compared using the correlation technique. The conclusion states that the phase congruency (PC) method is a powerful tool such that it has the ability to distinguish similar palmprints.

In [16], Qiang Zhang, el at. proposed approach based on utilizing Maximally Stable Extremal Region (MSER) detector and Gabor filter decomposition approach, in addition to phase congruency (PC) algorithm. Performance of the proposed approach was compared to the classical SIFT one using scenes with different scales. Results showed that concerning the advantages and help of phase congruency (PC) algorithm, the performance is better than the traditional MSER and affine-SIFT (ASIFT) methods. Also, the proposed method has a higher computation efficiency and robustness. A.F. Cinar, et al. in [17] used the phase congruency (PC) algorithm in the field of solid mechanics

concerning the fracture mechanics of cracks in order to study the behavior of cracks. The approach's accuracy is estimated and evaluated comparing to the conventional methods. Results showed that the phase congruency (PC) -based approach has high accuracy and robustness to noise. Clive Trenton in [18] used the phase congruency (PC) algorithm in the field space processing. The images are processed at high speeds in conjunction with FPGA implementation to provide a detection tool for space debris. Finally; he concluded that the effectiveness configuration of phase congruency (PC) implementation can properly satisfy an accurate offline analysis concerning a full-frame image.
Yuming Xiang, el at in [19] develop a SAR phase congruency edge detector (SAR-PC) by combining the ratio-based detectors and the phase congruency (PC) algorithm. This enhancement is performed starting with improving the model of SAR images local energy followed by an estimation of a new level of noise. Results depicted that the developed approach for detection of edges has a high robustness to the speckle noise and provides a consecutive response concerning edges. In [20], the authors propose a combination of MMPC-Lap detector and a descriptor based on phase congruency named local histogram of orientated phase congruency (LHOPC). Testing of various remote sensing images demonstrates that the proposed method has a high performance compared to the state-of-the-art. Finally, G. Mabuza-Hocquet, F. Nelwamondo in [21] utilized a combination of Phase Congruency (PC) and harris algorithms. They tried to enhance the process of iris recognition for the biological information system applications. The used sensor was a camera where the distance to object is very small (few meters) and the output is an intensity image of small size (hundreds of pixels) such that the target occupies a relatively large area inside the tested image. All detected features (inliers and outliers) were used without reduction process concerning the outliers which affect the result accuracy. Finally, the approach output is a binary template representing a feature vector of length 512-bits having the detected features location.
On the other side, the proposed method is used to enhance the image registration process as a remote sensing application. The used sensor is a radar where the distance to object is hundreds of kilometers and the output is a complex image of huge size (thousands / millions of pixels) such that the target occupies a relatively very small area inside the tested image. All features are detected including inliers and outliers, then; performing a reduction process for outliers to enhance the result accuracy. Finally, the output of the approach is a matrix of size MxN representing a registered image. SAR-PCH corner detector provides a reasonable output compared to that of conventional detectors (minimum eigenvalues, FAST, and harris) and it is a highly localized tool for feature detection.

3. Phase Congruency (PC) Algorithm

Many of image pre-processing approaches mainly rely on the power of correct detection, localization, and matching where the local features has the most important. Solving the issue of correct detecting and localization requires a robust tool which has high invariance to lightening and scaling. PC acts as a low-level operation for feature detection considering the ability of getting a reasonable output to be applied for proceeding levels of operations. Having an invariant feature, along broad ranges under different conditions of capturing the image, is a vital step such that it provides a robust material for achieving proceeding operations. The feature detection prime target is obtaining invariant feature considering variations of illuminations, texture, and scaling where considering feature as a keypoint depends on the pre-defined threshold value [1-11,13,22-25].
PC approach uses information provided by image representation in frequency domain. This is the strongest PC advantage where the feature is made out at a certain point where the components of Fourier having maximum phase, taking into account the local energy (E) calculations which is dimensional amount and proportional to PC measurements. PC values are in the range from 0:1 where value 0 indicates that no congruency and exemplary congruency for value 1. This dimensional measure gives the ability to select features prior image construction depending on the predetermined threshold value.

PC, itself, has a limitation as [13-16,22-27]:

1) it is highly affected by noise since it has a normalized amount;

2) it depends mainly on the Fourier components (A_n) amplitudes at the investigated feature (x) where the summation of A_n over point (x) may be: a) very small such that it tends to be 0 or b) only one A_n component exists such that it equals E(x). So; the spread and amplitude of A_n affect mainly on PC calculation where E(x) at point (x) has a direct relationship to PC as demonstrated later. For these two issues, PC value will be 0 for very small values of A_n or 1 for only one A_n component exists. Hence, PC estimations will be insignificant and inaccurate since its calculations depends on A_n. So, frequencies expansion plays an important role where PC measurements are mainly estimated based on A_n.
3) not providing accurate localization for the feature.

There is a relationship between PC and (E) where a model of local energy assumes that the feature is made out at the certain point where A_n have maximum phases such that PC calculations at any angle provides a distinctly keypoint. Fig. 1 demonstrates how to use components of Fourier chain to make up triangular and square waveforms.

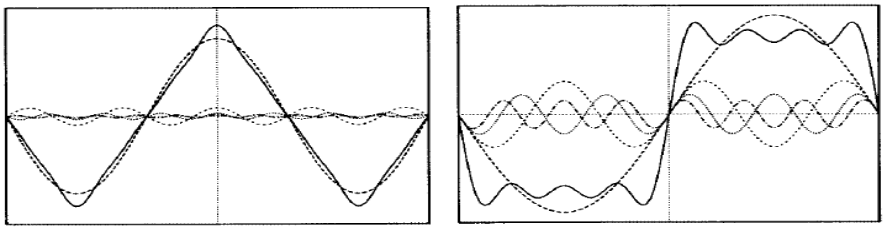

(a) (b)

Fig. 1. Making up of (a) triangular and (b) square waveforms

W.r.t 1-D signal I(x), PC function related to the expansion of Fourier at feature x will be estimated as [13,17,22-25,28].

$$s(x) = \sum_{n=0}^{\infty} \frac{1}{(2n+1)} sin[(2n+1)x + \phi] \tag{1}$$

$$PC(x) = max_{\overline{\phi}(x)\in[0,2\pi]} \frac{\sum_n A_n cos(\phi_n(x) - \overline{\phi}(x))}{\sum_n A_n} \tag{2}$$

where A_n is the n^{th} Fourier component's amplitude, $\phi_n(x)$ is the Fourier component's phase at location x, and $\overline{\phi}(x)$ is the amount of weighted mean local phase maximizing. The points having maximal PC can be estimated by direct looking for the peak position of E at point (x) as [22-25]

$$E(x) = \sqrt{F^2(x) + H^2(x)} \tag{3}$$

where F(x) is I(x) without DC composition and H(x) is F(x) Hilbert transform, then; E(x) can be estimated as [18,22-25,29]

$$E(x) = PC(x) \sum_n A_n \tag{4}$$

So, the local energy function (E) is direct proportion to PC measurements. Before normalization process, the noise will be estimated and then subtracted from E(x). This process reduces the noise response and PC will be modified as [13-16,19,22-27,29]

$$PC(x) = \frac{\lfloor E(x) - T \rfloor}{\sum_n A_n(x) + \varepsilon} \tag{5}$$

where the proper account of (ε) relies on the accuracy of information extraction and used to avoid dividing by zero. The ringed amount $\lfloor E(x) - T \rfloor$ equals to itself at moment having a positive value and zero elsewhere. So, considering point (x) during the calculations is related to the noise level. Frequency spread acts as an important parameter where PC point is considerable when occurring along an extended frequencies range. Since smoothing process minimizes the high components of frequency causing reduction of expansion of frequency, so; weight function W(x) should be added to weight PC by counting the aggregate of A_n and divided by the largest A_n. So, the spread function s(x) will be as

$$s(x) = \frac{1}{N}\left(\frac{\sum_n A_n(x)}{A_{max}(x) + \varepsilon}\right) \tag{6}$$

where N is overall number of scales and Amax(x) is largest frequency component at x, thus [13,19-25,29]

$$PC(x) = \frac{W(x)\lfloor E(x) - T \rfloor}{\sum_n A_n(x) + \varepsilon} \tag{7}$$

PC localization problem is still existing after spread function modifications because there is a proportional relation between E(x) and divergence ΔΦ(x) of phase angle ϕn(x) from total average of phase angle $\overline{\phi}(x)$ is given as

$$\Delta\Phi(x) = cos(\phi_n(x) - \overline{\phi}(x)) - \left|sin(\phi_n(x) - \overline{\phi}(x))\right| \tag{8}$$

Thus,

$$PC(x) = \frac{\sum_n W(x)\lfloor A_n(x)\Delta\Phi_n(x) - T \rfloor}{\sum_n A_n(x) + \varepsilon} \tag{9}$$

where T is the estimated effect of noise. To extend PC algorithm to 2-D images, thorough studies of (E) w.r.t 2-D image were discussed. Applying PC approach for 2-D images requires applying it for each direction separately and finally combining the results. Final PC equation at location (x) will be given as [13,19-25,28-30].

$$PC(x) = \frac{\sum_o \sum_n W_o(x)\lfloor A_{no}(x)\Delta\Phi_{no}(x) - T_o \rfloor}{\sum_o \sum_n A_{no}(x) + \varepsilon} \tag{10}$$

where (o) represents the orientation index where the energy normalizing process to construct PC is carried out after combining overall local energies for all possible orientations. Also, the noise compensation is achieved independently for each orientation. In order to implement the PC algorithm, the required procedures start by applying quadrature pairs of wavelets filters over number of orientations, equals 6, and number of different scales, equals 4, for each point in the image. This process will be performed for x and y directions independently providing the frequency data. Then, the PC covariance matrix will be calculated as

$$G = \begin{bmatrix} \sum PC_x^2 & \sum PC_xPC_y \\ \sum PC_xPC_y & \sum PC_y^2 \end{bmatrix} \tag{11}$$

where PC_x and PC_y are PC components in x and y directions where summation is to acquire the values for all orientations. Having large values of minimum PC moments (m) and maximum PC moments (M) as shown in Fig. 2 indicate that the point has a powerful being a corner for (m) values and prominence of point surely to be edge for (M) values [13-30].

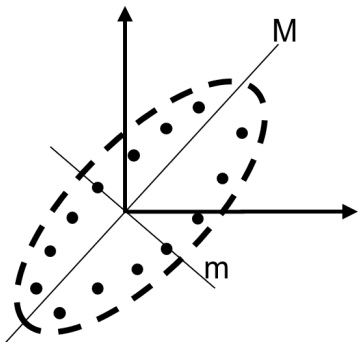

Fig. 2. Illustration of maximum and minimum PC moments

4. Harris Corner Detector

Harris detector [31] is a uni-scale detector that based on intensities derivatives to handle moravec's detector [32] limitations by acquiring the intensity variations for all different orientations. Its utilization is mainly for images with gray scales and it can be counted as a mishmash of corner and edge detectors. The principle idea is the eigenvalues estimation for regions having small patches, then utilizing the greatest eigenvalues to specify a predefined function combined with a threshold to examine the corners as shown in figure 1. The local directional matrix is used to detect the direction of fastest and slowest variations for the feature orientation. Image gradients (Ix, Iy) in x and y directions will be estimated for all pixels resulting a correlation matrix (M) [8-12,31]:

$$M = \begin{bmatrix} I_x^2 & I_x I_y \\ I_x I_y & I_y^2 \end{bmatrix} \tag{12}$$

All matrix's components are smoothed improving detector's robustness. As mentioned above, estimations of eigenvalues are the main essence such that using it combined with a certain threshold value to depict the feature to be a corner or not. This is known as pixel score (Rs) which can be determined as [8-12,31]:

$$R_s = \lambda_1 \lambda_2 - k(\lambda_1 + \lambda_2)^2 \tag{13}$$

where λ1 and λ2 are eigenvalues of (M) and k is the detector sensibility agent whose value is within range 0.04:0.06. Pixel is considered to be a corner if both λ1 and λ2 are high as shown in figure 3(a). Computational cost of eigenvalues estimation is high, so that an enhancement will be applied using trace and determinant of matrix (M) providing oncoming relationship to estimate (Rs) as [8-10, 31].

$$R_s = det(M) - k(trace(M))^2 \tag{14}$$

An enhancement over Harris detector was proposed allowing utilization for color data [2, 6-10]. Shi and Tomasi [33] developed an optimization approach based on Harris method permitting the minimum eigenvalues utilization for differentiating keypoints and hence controls and facilitates the cost computations of Harris detector. When (Rs) is higher than pre-determined threshold value, keypoint is a corner as shown in figure 3(b) where (Rs) is estimated as [8-10, 33].

$$R_s = \min(\lambda_1, \lambda_2) \tag{15}$$

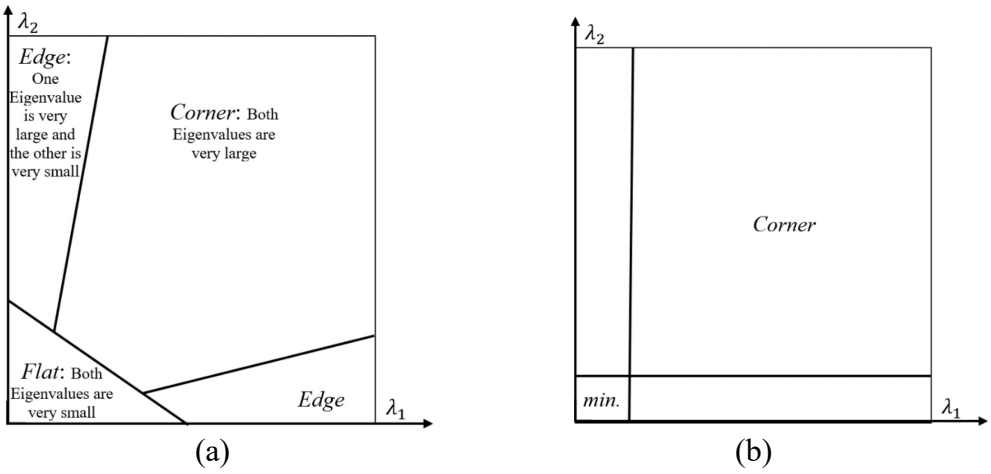

Fig. 3. Principle idea of both a) Harris and b) Shi, Tomasi corner detectors

Harris detector has various privileges as being invariant to rotation, illumination, and translation changes. Also, it has high stability, rotational invariant repeatability, informativeness, accurately localized. In spite of all these, Harris detector has a limitation as sensitivity to noise, cost computations, and variant to high scale variations. Harris Laplace and Harris Affine were proposed acting as an affine invariant corner detector designed to multi-scale operations. This gains the property of robustness to transformations from perspective types since it is invariant to affine ones. The gist thought behind is a mixture of Harris and a gaussian scale space allowing the features detection over a various scale's levels. They have properties of providing a representative set of points with highly repeatable in the scale dimension and being insensitive to scale, illumination, rotation, and noise variations. Usage limitations are that providing a reduced redundant key point and not efficient for affine issues. Also, an enhancement depending on Harris was performed permitting distinguishing neighborhoods of key points since edges have the stability property for being image features over multiple viewpoints; scales; and illumination variations [8-12].

5. Methodology

The illustrated registration method is a mix of ABM and FBM techniques. It will be carried out starting by cross-correlation method as ABM technique performing the coarse registration and then applying result to SAR-PCH corner detector to perform the fine registration where processing of PC images using the Harris detector is performed such that at first; PC image will be acquired using PC algorithm and then applied to Harris detector to get the corner points. Second; using Random Sample Consensus (RANSAC) algorithm [34] to eliminate the undesired corner points in order to have the correct transformation matrix. Finally; the sensed image will be interpolated.

5.1 Proposed Framework

A smoothing filter, gaussian-kernel filter, is used as a first step to reduce the noise effect. Both master and slave images are processed as follows:
First, as shown in figure (4); performing a directly applying the FBM methods to the input images, the proposed SAR-PCH detector in addition to the other mentioned ones. Then, using Random Sample Consensus (RANSAC) algorithm [34] to reduce the undesired corner points in order to have the correct transformation matrix. It is very important to mention that the depicted workflow shown in Fig. 4 is used to investigate the behavior of SAR-PCH corner detector with respect to the other.
Second, Fig. 5 represents the overall workflow of the proposed method. After getting slave and master images, shift between input images; PSNR; and MSE are estimated before initiating process of registration to find out the performance of proposed approach. The depicted method is mainly dependent on a combination between ABM and FBM techniques. First; ABM technique, represented in correlation method, will be applied performing the stage of coarse registration. A shifted slave image will be generated, and estimations related to shift between input images, PSNR, and MSE after

coarse registration will be calculated. Second; FBM technique, represented in SAR-PCH corner detector, will be carried out acting as fine registration stage. SAR-PCH will generate a number of matched points in both master and shifted slave images. These points are classified as inliers (desired) and outliers (undesired). The extracted matched points will be applied to RANSAC algorithm, as shown in figure 6, to generate a geometric transformation matrix satisfying the cost function of RANSAC to eliminate the outliers points which will affect the performance of transformation matrix generation and only pick out the inliers points which are most correctly matched points between the input images to increase the fineness of transformation matrix performing better fine registration. So, RANSAC can be considered as an optimization approach.
Third, Fig. 7 represents the same overall workflow of the proposed method as shown in Fig. 5, but; adding a speckle noise to both master and slave image of first and fourth pairs as examples for both cases, simulated complex images and real amplitude images. The added speckle noise has zero mean and different values of variance. that is to investigate the performance of the proposed method in case of a sever noise existence in order to verify the effectiveness of the proposed approach where it overcomes the Harris noise sensitivity limitation.

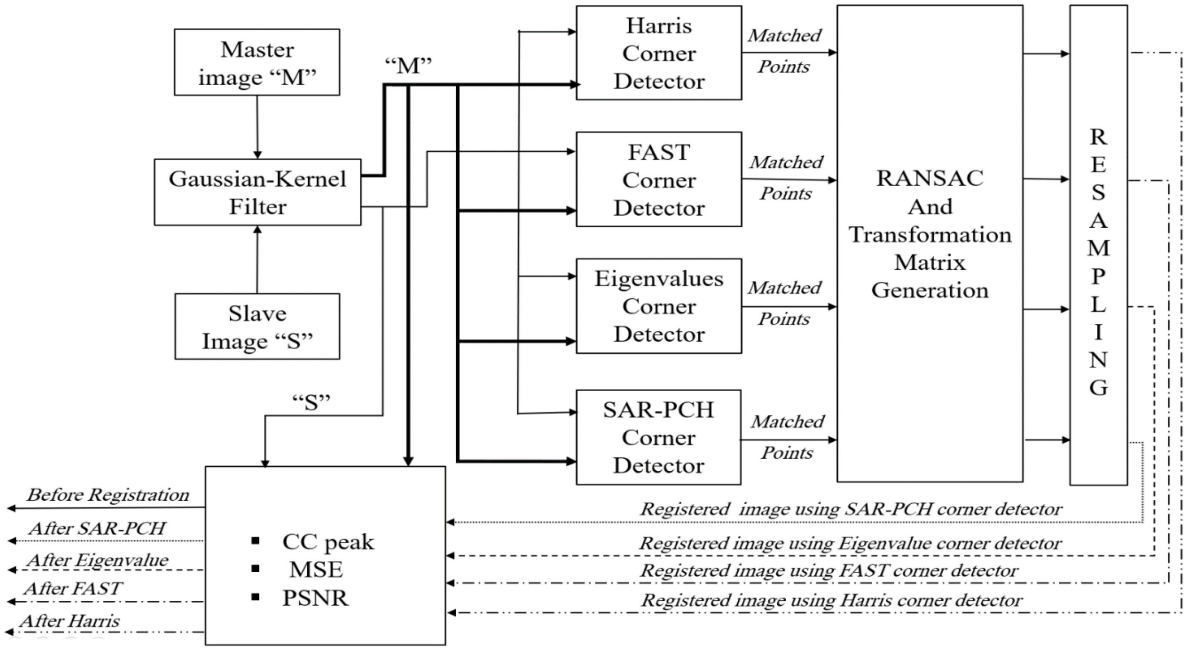

Fig. 4. Illustration of directly applying FBM method

Features from Accelerated Segment Test (FAST) [35] was proposed based on [36] acting as detector used for one scale. Interest point is extracted by utilizing a circle, known as Bresenham, having 16 pixels diameter concerning each pixel. Then performing a test for the whole pixels of the image will be accomplished employing a cramped window size in addition to the reality that somewhat of pixels are investigated, not all pixels [2-12]. Finally, transformation matrix is required to interpolate the shifted slave image produced from ABM method.

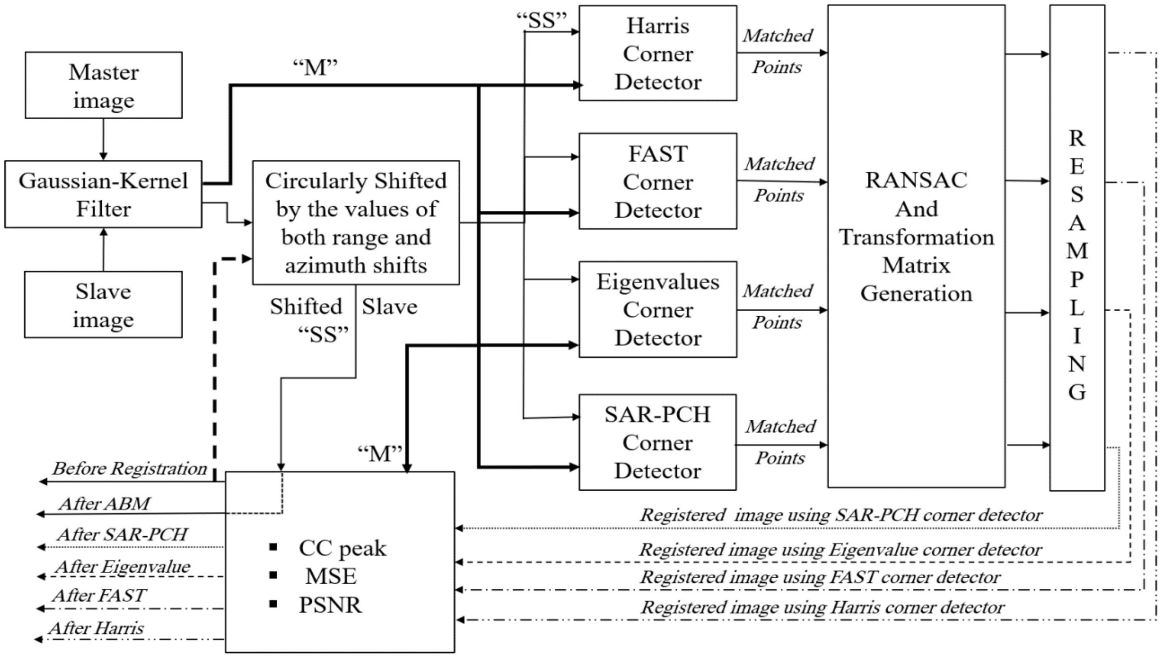

Fig. 5. General workflow of the proposed registration method

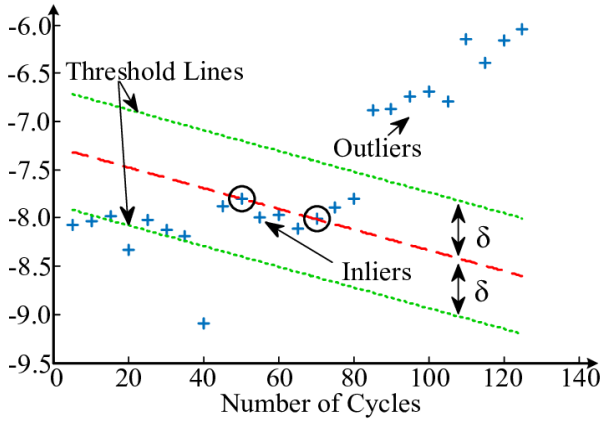

Fig. 6. Description of RANSAC Concept

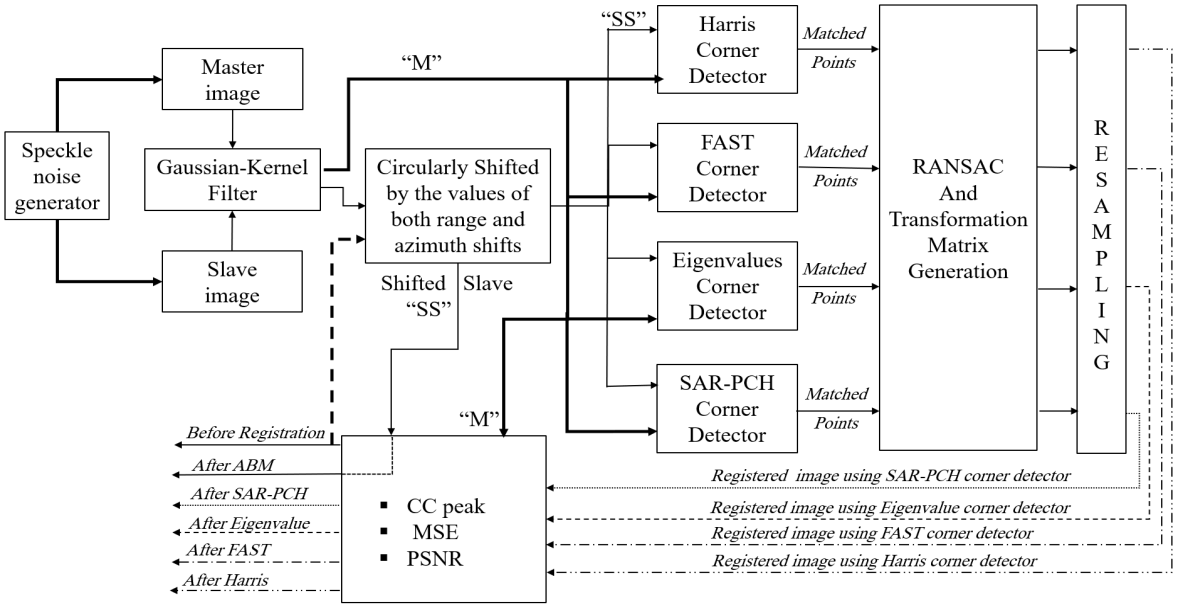

Fig. 7. General workflow of the proposed registration method in case of noise existence

5.2 Experimental Dataset

Four pairs of images dataset are tested including simulated and real images. Images are acquired from various sensors having multiple sizes as presented in Table 1 where pair no. 1 represents a simulated image for flat area as shown in Fig. 8. Pair no. 2 represents a real image for part of China and pair no. 3 represents a real image for Las Vegas; USA as shown in Fig. 9 and Fig. 10 respectively. Finally, pair no. 4 represents a real image for Aswan Dam; Egypt as shown in Fig. 11. Table 2 presents the threshold value of the used detectors concerning each pair of images.

Table 1. Specifications of Working on Data set

Working on data set				
Pair No.	(1)	(2)	(3)	(4)
Image Type	Simulated	Real		
Sensor	-	ERS 1, 2	ERS 1, 2	Terra-X
Location	-	Part of China	Las Vegas, USA	Aswan Dam, Egypt
Pixel Shift	0, 1	0, 0	199, 6	60, -40
Data type	Complex	Amplitude	Complex	Amplitude
Size	1502*1148	9000*2500	3000*3000	1800*3600

Table 2. Threshold value of SAR-PCH and the used detectors

Pair No.		(1)	(2)	(3)	(4)
Threshold of used detectors	Harris	1.0e-08	1.0e-06	1.0e-06	1.0e-06
	Eigenvalues	1.0e-06	1.0e-06	1.0e-06	1.0e-06
	FAST	5	1200	100	500
	SAR-PCH	1.0e-08	1.0e-08	1.0e-06	1.0e-06

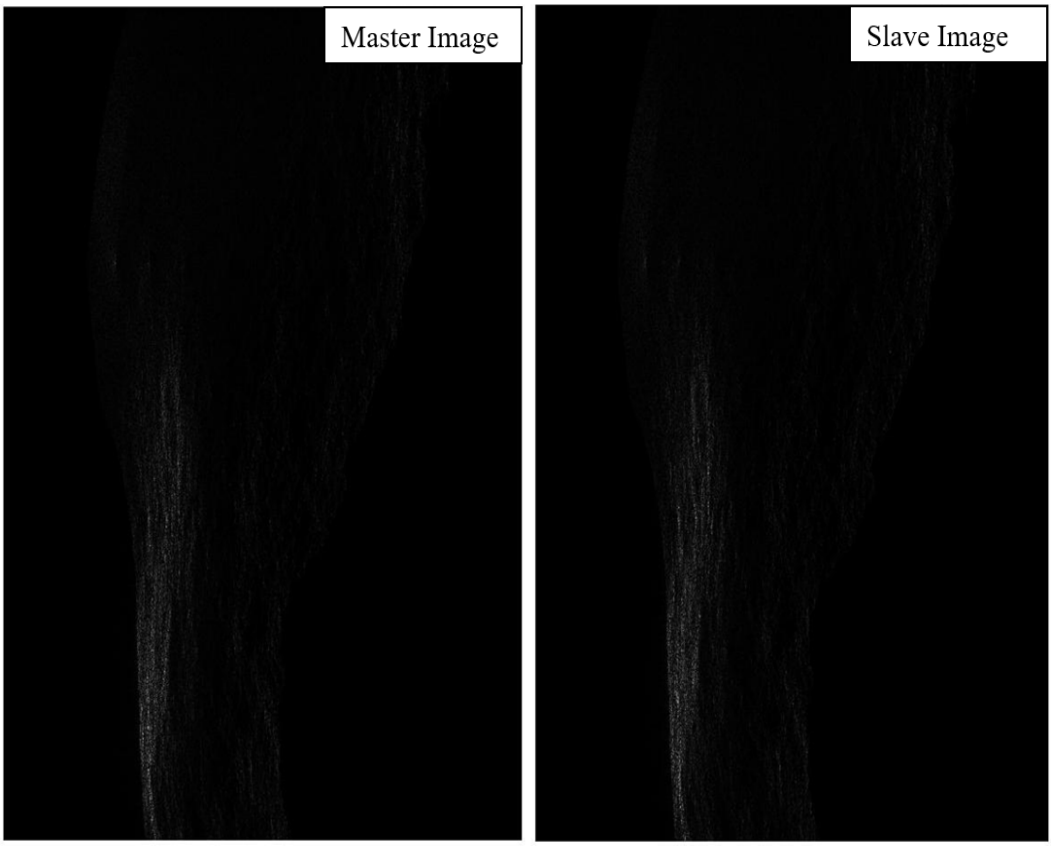

Fig. 8. 1st pair of SAR images (simulated)

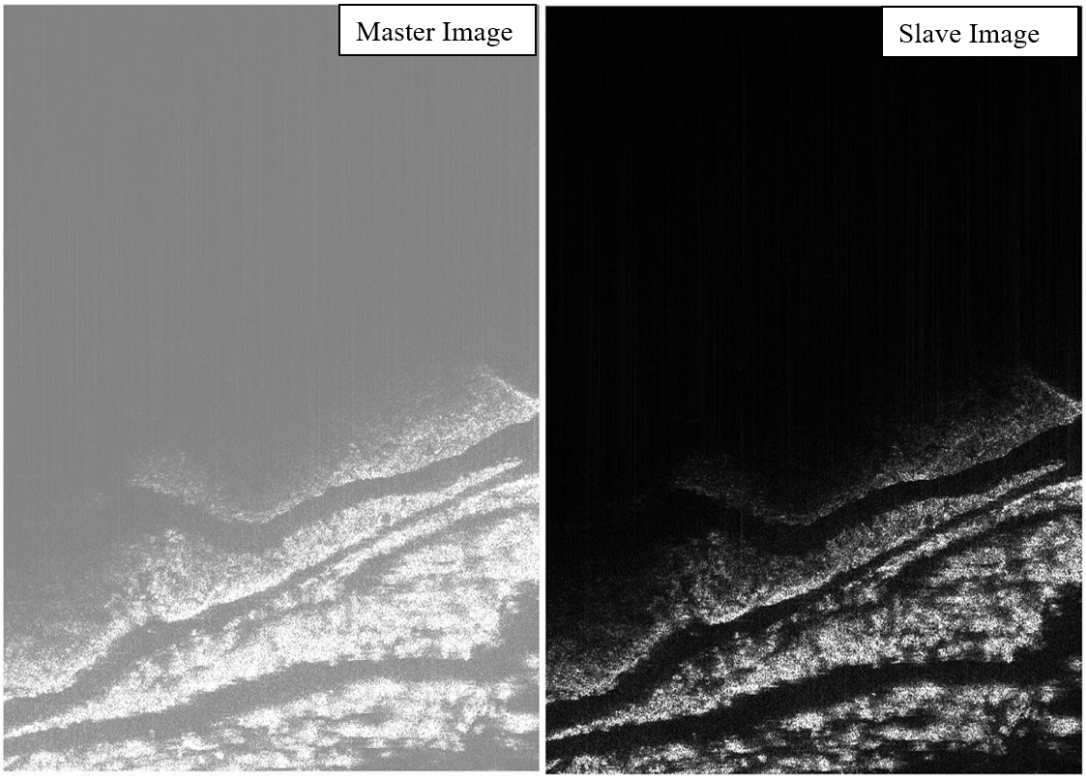

Fig. 9 2nd pair of SAR images (real)

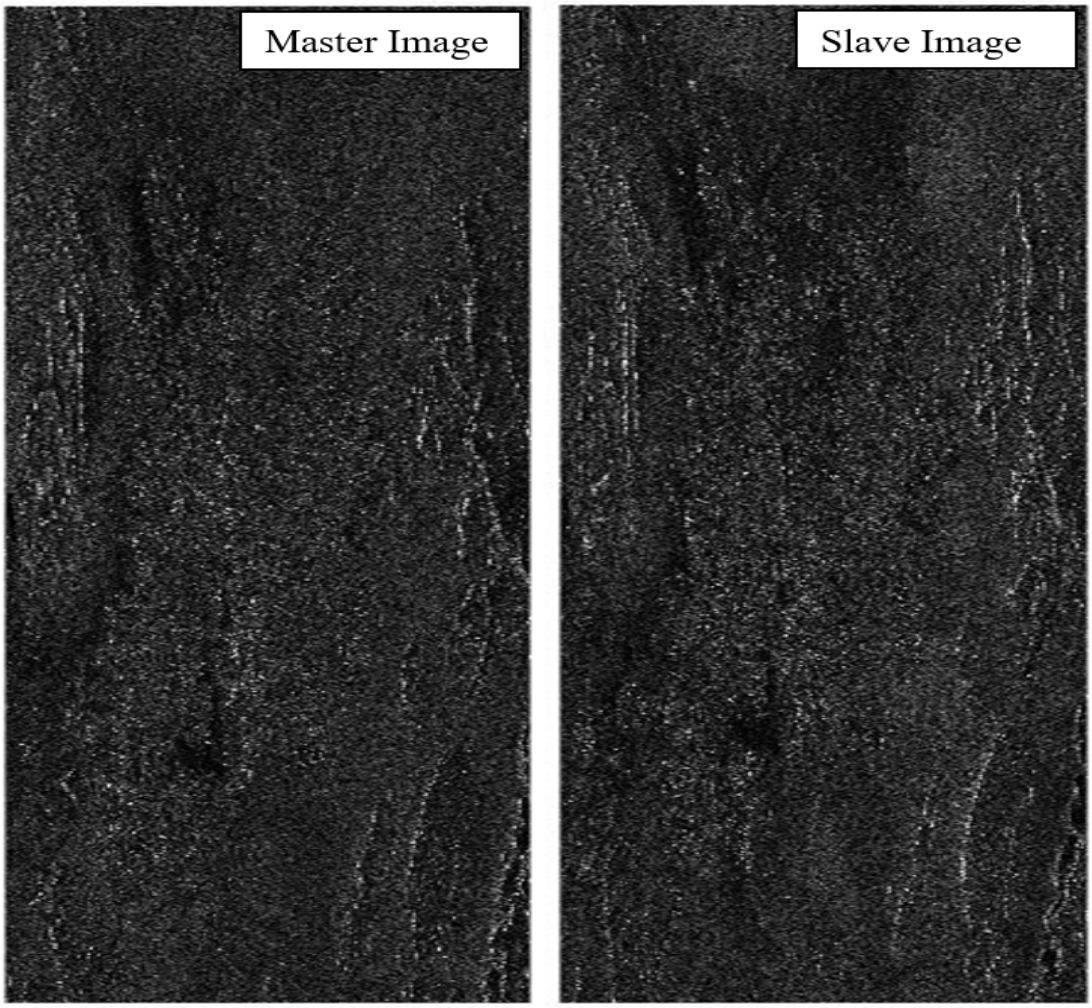

Fig. 10. 3rd pair of SAR images (real)

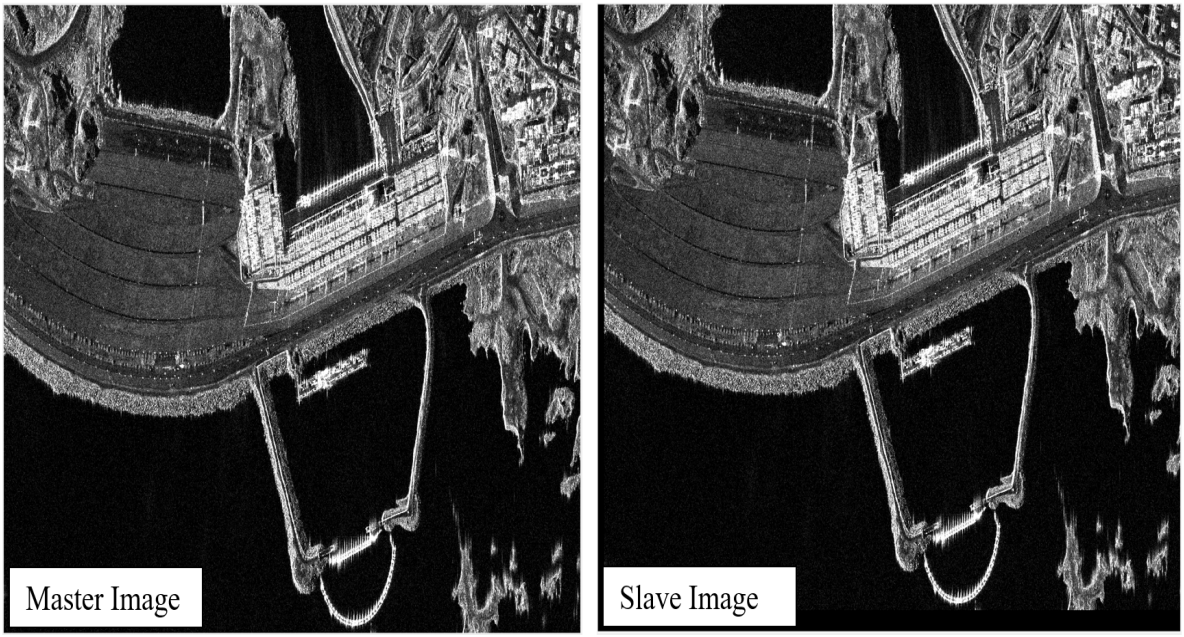

Fig. 11. 4th pair of SAR images (real)

5.3 Evaluation of the proposed approach

In order to evaluate the performance of the proposed corner detector, a widespread utilized detector [31], [33], and [35] are used to evaluate the depicted approach execution. Before starting evaluation

step for the accuracy of registration process, it is important to have a knowledge about the type of payload or sensor which captured the images. There are two cases, the first case concerns the capturing process using the same sensor, known as "same modality / mono-modal", where the other concerns the usage of different sensors and known as "different modality / multi-modal". That is to correctly choose the evaluation strategy. There are many metrices to evaluate the performance of the registration process. The most commonly used metrices are peak signal-to-noise ratio (PSNR), root mean square error (RMSE), and coherence image or coherence factor. The selection of any method is related to the user's choice since these metrices are a measuring tools for evaluating the performance of overall registration process in order to depict the behavior of the used approach for feature detection.

Suppose having two images, the master image (I_1) and the sensed image (I_2). Applying the forward and backward registration processes using a mapping functions (f) and (g) respectively as shown in Fig. 11. If there is no error after performing both forward and backward registration processes, point (z\) coincides with point (z).

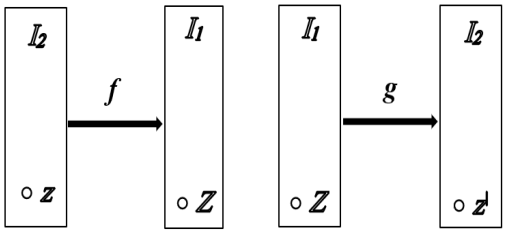

Fig. 11. Illustration of RMSE calculations for both: (a) forward and (b) backward processes

In case of error, an offset between points (z\) and (z) occurs. Closer points mean that the registration will be more accurate. After forward and backward transformations and for (N) keypoints in the sensed image (I_2), then root-mean-square error will be given by

$$RMSE = \sqrt{\frac{1}{N}\sum_{i-1}^{N}\|z_i - g(f(z_i))\|^2} \tag{16}$$

Finally, RMSE has a meaningful for both cases of mono-modal and multi-modal where the smaller value of RMSE reflects a high accuracy. Mean square error (MSE) is also used as a measure tool where the average squared difference between the values of both reference and sensed pixels and it is calculated as:

$$MSE = \frac{1}{N}\sum[R(i,j) - S(i,j)]^2 \tag{17}$$

where R and S are the reference and sensed images of the same size, N is the total number of pixels, and i and j are the numbers of rows and columns.

The performance of the registration process can be evaluated using the coherence image, may be called coherence map. Coherence image can be used for both cases, mono-modal and multi-modal images. Suppose we have two complex SAR images, the master image (I_1) whose pixels are denoted by (P_1) and the sensed image (I_2) whose pixels are denoted by (P_2). Since the SAR image is a complex, then; each pixel in both master and sensed images is given as a complex form containing real part (R) and imaginary part (I) such that

$$P_1 = R_1 + jI_1 \tag{18}$$

$$P_2 = R_2 + jI_2 \tag{19}$$

the coherence factor (γ) is a complex number and estimated using the following relation between pixels (P_1) and (P_2) as

$$\gamma = \frac{E[p_1 p_2^*]}{\sqrt{E[p_1 p_1^*]E[p_2 p_2^*]}} \tag{20}$$

where the amount ($E[p_1 p_2^*]$) represents the ensembled average energy over a window of size (m x n) and (*) is the complex conjugate. To evaluate the accuracy of the registration process, |γ| is usually used. For SLC-SAR images and over a window of size (m x n), the coherence factor |γ| can be represented as

$$|\gamma| = \frac{|E[p_1 p_2^*]|}{\sqrt{E[|p_1|^2]E[|p_2|^2]}} = \frac{|\sum_{MxN}(R_1 + jI_1)(R_2 + jI_2)|}{\sqrt{\sum_{MxN}(R_1^2 + I_1^2)\sum_{MxN}(R_2^2 + I_2^2)}} \tag{21}$$

Coherence factor |γ| is within range (0:1) whereas its value increases, this indicates high accuracy of registration process and vice versa. Also; coherence factor |γ| is the most commonly utilized measurement for evaluation of SAR image registration performance. This coherence value is improved by minimizing all image distortion which affects the intensities of pixels as speckle noise. The speckle phenomena, itself, may be used to accelerate (not improve) the procedures of coherence estimation depending on the speckle similarity.
Peak Signal-to-Noise Ratio (PSNR) is calculated as

$$PSNR = 10\log_{10}\left(\frac{S_{max}^2}{MSE}\right) \tag{22}$$

where Smax is the maximum pixel value of the sensed image and MSE is a measurement for the average squared difference between the values of both reference and sensed pixels.

5.4 Results

The demonstrated dataset allows to examine two forms of tested SAR images, the first one is the simulated and real images accompanied by approximately no shift while the second form is the real images accompanied by a little high shift. The results are calculated during the overall co-registration process; i.e. before, after applying ABM, and after applying FBM. Applying a cross-correlation method before SAR-PCH corner detectors improves the results. So, a combination of these two area-based matching (ABM) methods is proposed. The results are as follows:
Concerning the first pair of images, the results are shown in Tables (3:6). It indicates the performance of two cases; first one is the usage of the proposed approach directly as FBM method and second is the usage of a combination of ABM method and SAR-PCH as FBM method. Each case has two phases, the first phase is performed without adding a speckle noise and the second phase is performed with adding speckle noise with zero mean and different values of variances. According to the proposed algorithm (combination between ABM and FBM) without adding a speckle noise, putatively matched points between the images; location of cross-correlation peak; and the coherence map during the overall procedures of the process are shown in Figures 12, 13, and 14 respectively.
Concerning the second pair of images, the results are shown in tables 7 and 8. It indicates the performance of two cases; first one is the usage of the proposed approach directly as FBM method and second is the usage of a combination of ABM method and SAR-PCH as FBM method. Each case is performed without adding a speckle noise. Relative to the proposed algorithm (combination between ABM and FBM) without adding a speckle noise, putatively matched points between the images and location of cross-correlation peak are shown in Figures 15 and 16 respectively. There are no results for the value of coherence factor since this value is based on the complex intensity value (real and imaginary) and this pair is gray-scale (absolute value not complex).
Concerning the third pair of images, the results are shown in Tables 9 and 10. It indicates the performance of two cases; first one is the usage of the proposed approach directly as FBM method and second is the usage of a combination of ABM method and SAR-PCH as FBM method. Each case is performed without adding a speckle noise. W.r.t the proposed algorithm (combination between

ABM and FBM) without adding a speckle noise, putatively matched points between the images; location of cross-correlation peak; and the coherence map during the overall procedures of the process are shown in Figures 17, 18, and 19 respectively.
Concerning the fourth pair of images, the results are shown in tables (11:14). It indicates the performance of two cases; first one is the usage of the proposed approach directly as FBM method and second is the usage of a combination of ABM method and SAR-PCH as FBM method. Each case has two phases, the first phase is performed without adding a speckle noise and the second phase is performed with adding speckle noise with zero mean and different values of variances. For the proposed algorithm (combination between ABM and FBM) without adding a speckle noise, putatively matched points between the images and location of cross-correlation peak are shown in Figures 20 and 21 respectively. There are no results for the value of coherence factor since this value is based on the complex intensity value (real and imaginary) and this pair is gray-scale (absolute value not complex).
Considering addition of speckle noise to the image pair number 1, Figures (22:27) shows samples of the output at different values of variances (0.01, 0.1, and 0.9) in case of using SAR-PCH directly as FBM method. This is the worst case since there is an existence of noise in addition to no usage for AMB method. As mentioned above, that is to investigate the performance of the proposed algorithm.

5.5 Analysis and Discussion

The images are exposed to Gaussian-Kernel filter to reduce the effects of noise which impedes detection and extraction of the keypoints. Tables 3:10 and Figures 12:21 show the experimental results where the proposed approach performance is compared to the traditional detectors as mentioned above. The proposed approach is a combination of cross-correlation approach as an area-based matching method in addition to SAR-PCH as a feature-based matching method. After coarse registration process, the value of the shift between the inputs equals (0,0), but a sub-pixel shift exists and not sensed. After fine registration process, the value of the shift between inputs equals (0,0) exactly. The performance of the proposed method will be very good concerning the images having extreme PSNR since the noise will have a less effect and this facilitates the process of features detection and extraction.
Applying a speckle noise causes a change of both PSNR and coherence values. As the value of speckle noise variances increases, the above-mentioned values decrease. So, there is an inverse relationship between the noise strength and the estimated values o PSNR and coherence factor. W.r.t the results of adding a noise, the performance of the proposed detector, SAR-PCH, is better than that of all traditional ones. Harris corner detector may reflect a higher value of coherence, but it is not a real value since the cross-correlation peak position between the master and registered images is not centered at the window. This verifies that the proposed detector, SAR-PCH, overcomes the limitations Harris detector where it is more sensitive to the noise. Also, the results show the performance considering high and sever PSNR values.
Finally, the proposed method, a combination of ABM and FBM methods, is used to enhance the image registration process as a remote sensing application. The used sensors are radar satellites where the distance to object is hundreds of kilometers and the output is a complex image of huge size (thousands / millions of pixels) such that the target occupies a relatively very small area inside the tested image. All features are detected including both inliers and outliers, then; performing a reduction process for outliers to enhance the result accuracy using the random sample consensus (RANSAC) algorithm.
The output of the approach is a matrix of size MxN representing a registered image. Results show that the proposed SAR-PCH corner detector provides a reasonable output compared to that of conventional detectors and it is a highly localized tool for features detection. SAR-PCH corner detector is used lonely as a feature-based matching method directly or combined with an area-based matching method.

Table 3. Experimental results of image pair No. 1,
Using SAR-PCH directly as FBM method

No added speckle noise		**Harris**	**FAST**	**Eigenvalues**	**SAR-PCH**
Before	Cross-correlation peak	0, 1			
	MSE	1.8154			
	PSNR	45.5410			
	Avgerage Coherence	0.8106			
FBM	No. of Matched Points	90	30	70	36
	Cross-correlation peak	0,0	0,0	0,0	0,0
	MSE	1.1255	1.1258	1.1257	1.1258
	PSNR	47.6174	47.6162	47.6166	47.6161
	Avgerage Coherence	0.8894	0.8893	0.8894	0.8893

Table 4. Experimental results of image pair No. 1, using the proposed approach
(combination of ABM method and SAR-PCH as FBM method)

No added speckle noise		**Harris**	**FAST**	**Eigenvalues**	**SAR-PCH**
Before	Cross-correlation peak	0, 1			
	MSE	1.8154			
	PSNR	45.5410			
	Avgerage Coherence	0.8106			
ABM	Cross-correlation peak	0, 0			
	MSE	1.1243			
	PSNR	47.6222			
	Avgerage Coherence	0.8896			
FBM	No. of Matched Points	90	30	70	36
	Cross-correlation peak	0,0	0,0	0,0	0,0
	MSE	1.1239	1.1242	1.1241	1.1243
	PSNR	47.6234	47.6222	47.6226	47.6222
	Avgerage Coherence	0.8896	0.8896	0.8896	0.8896

Table 5. Experimental results of image pair No.1, using the proposed approach (combination of ABM method and SAR-PCH as FBM method)

Added a speckle noise with zero mean and different values of variances							
Variance of Speckle noise	*Similarity Metrices*	*Before*	*ABM*	*Harris*	*FAST*	*Eigen-values*	*SAP-PCH*
0.01	A	0,1	0,0	98,0	95,0	0,51	0,0
	B	1.8160	1.1508	1.9334	1.9610	1.8553	1.9000
	C	45.5396	47.5206	45.2676	45.2061	45.4468	45.3433
	D	0.8048	0.8829	0.7602	0.8364	0.6102	0.6132
0.05	A	0,1	0,0	0,0	94,0	-1,1	0,0
	B	1.8182	1.2426	1.8784	1.8545	1.8805	1.8441
	C	45.5343	47.1877	45.3930	45.4486	45.3880	45.4729
	D	0.7816	0.8562	0.5789	0.5671	0.6205	0.6648
0.07	A	0,1	0,0	0,79	57,-39	18,0	0,0
	B	1.8203	1.2821	1.8421	1.8471	1.8607	1.8786
	C	45.5294	47.0516	45.4776	45.4659	45.4341	45.3923
	D	0.7701	0.8430	0.4781	0.5064	0.6505	0.5958
0.09	A	0,1	0,0	0,0	-1,1	95,0	00
	B	1.8202	1.3144	1.8982	1.8370	1.9469	1.8759
	C	45.5296	46.9436	45.3473	45.4897	45.2373	45.3988
	D	0.7592	0.8303	0.6078	0.6382	0.7968	0.5634
0.1	A	0,1	0,0	0,80	0,0	0,0	0,0
	B	1.8191	1.3300	1.8664	1.8519	1.8440	1.9588
	C	45.5322	46.8923	45.4208	45.4547	45.4732	45.2108
	D	0.7538	0.8240	0.8666	0.6395	0.6307	0.8224
0.5	A	0,1	0,0	0,1	0,0	0,-74	0,0
	B	1.8392	1.5911	1.8309	1.8667	1.8361	1.8611
	C	45.4844	46.1140	45.5042	45.4201	45.4919	45.4331
	D	0.5935	0.6429	0.5650	0.4921	0.5453	0.5639
0.7	A	0,1	0,0	-1,68	89,93	89,90	89,93
	B	1.8360	1.6052	1.8245	1.8559	1.8564	1.8510
	C	45.4921	46.0775	45.5194	45.4453	45.4440	45.4568
	D	0.5808	0.6279	0.4475	0.5834	0.5812	0.5746
0.9	A	0,1	0,0	72,78	0,0	0,0	0,0
	B	1.8340	1.6085	1.8214	1.8397	1.8383	1.8287
	C	45.4968	46.0738	45.5268	45.4834	45.4865	45.5095
	D	0.5789	0.6263	0.5569	0.5305	0.5148	0.5340

A ---- Location of Cross-correlation Peak
B ---- Mean Square Error (MSE)
C ---- Peak Signal-to-Noise Ratio (PSNR)
D ---- Average Coherence Factor

Table 6. Experimental results of image pair No.1,
Using SAR-PCH directly as FBM method

Added a speckle noise with zero mean and different values of variances							
Variance of Speckle noise	*Similarity Metrices*	*Before*	*ABM*	*Harris*	*FAST*	*Eigen-values*	*SAP-PCH*
0.01	A	0,0	-	0,0	-87,59	0,0	0,0
	B	1.8161	-	1.8653	1.8283	1.8585	1.9250
	C	45.5394	-	45.4233	45.5103	45.4393	45.2866
	D	0.8047	-	0.6906	0.5451	0.6886	0.7098
0.05	A	0,1	-	0,61	0,-88	-7,-55	0,0
	B	1.8175	-	1.8342	1.8446	1.8310	1.9484
	C	45.5360	-	45.4963	45.4718	45.5040	45.2340
	D	0.7815	-	0.5472	0.7479	0.4816	0.7628
0.07	A	0,1	-	0,0	48,20	2,99	0,0
	B	1.8186	-	1.8518	1.8258	1.8389	1.8574
	C	45.5335	-	45.4548	45.5162	45.4851	45.4418
	D	0.7702	-	0.6351	0.6862	0.6509	0.6450
0.09	A	0,1	-	-1,1	0,0	87,9	0,0
	B	1.8211	-	1.8855	1.8456	1.8309	1.9273
	C	45.5274	-	45.3766	45.4694	45.5041	45.2812
	D	0.7590	-	0.6106	0.5997	0.6491	0.7151
0.1	A	0,1	-	-83,1	1,0	-1,1	0,0
	B	1.8230	-	1.8368	1.8654	1.8907	1.8550
	C	45.5229	-	45.901	45.4230	45.3647	45.4474
	D	0.7532	-	0.6354	0.5924	0.5768	0.6258
0.5	A	0,1	-	84,-94	0,-81	87,97	0,0
	B	1.8397	-	1.8328	1.8397	1.8470	1.9079
	C	45.4834	-	45.4995	45.4833	45.4662	45.3252
	D	0.5937	-	0.5225	0.5699	0.5397	0.6115
0.7	A	0,1	-	95,0	86,-98	98,81	0,0
	B	1.8391	-	1.9419	1.8355	1.8698	1.8516
	C	45.4847	-	45.2485	45.4933	45.4129	45.4554
	D	0.5801	-	0.6816	0.5347	0.7196	0.5313
0.9	A	0,1	-	78,0	-1,1	0,0	0,0
	B	1.8344	-	1.8585	1.8832	1.8715	1.8541
	C	45.4958	-	45.4392	45.3818	45.4090	45.4496
	D	0.5790	-	0.4975	0.5346	0.5335	0.5558

A ---- Location of Cross-correlation Peak
B ---- Mean Square Error (MSE)
C ---- Peak Signal-to-Noise Ratio (PSNR)
D ---- Average Coherence Factor

Table 7. Experimental results of image pair No. 2,
Using SAR-PCH directly as FBM method

No added speckle noise		Harris	FAST	Eigenvalues	SAR-PCH
Before	Cross-correlation peak	0, 0			
	MSE	1.4457			
	PSNR	46.5300			
FBM	No. of Matched Points	156	393	134	73
	Cross-correlation peak	0,0	0,0	0,0	0,0
	MSE	1.4507	1.4514	1.4501	1.4481
	PSNR	46.5150	46.5130	46.5170	46.5227

Table 8. Experimental results of image pair No. 2, using the proposed approach
(combination of ABM method and SAR-PCH as FBM method)

No added speckle noise		Harris	FAST	Eigenvalues	SAR-PCH
Before	Cross-correlation peak	0, 0			
	MSE	1.4457			
	PSNR	46.5300			
ABM	Cross-correlation peak	0, 0			
	MSE	1.4457			
	PSNR	46.5300			
FBM	No. of Matched Points	156	393	134	73
	Cross-correlation peak	0, 0	0, 0	0, 0	0, 0
	MSE	1.4507	1.4514	1.4501	1.4481
	PSNR	46.5150	46.5130	46.5170	46.5227

Table 9. Experimental results of image pair No. 3,
Using SAR-PCH directly as FBM method

No added speckle noise		Harris	FAST	Eigenvalues	SAR-PCH
Before	Cross-correlation peak	199, 6			
	MSE	1.8465			
	PSNR	88.3482			
	Avgerage Coherence	0.8070			
FBM	No. of Matched Points	46	9	51	20
	Cross-correlation peak	0,0	0,0	0,0	0,0
	MSE	1.3144	1.3148	1.3146	1.3147
	PSNR	89.5199	89.5241	89.5235	89.5290
	Avgerage Coherence	0.8469	0.8469	0.8468	0.8469

Table 10. Experimental results of image pair No. 3, using the proposed approach (combination of ABM method and SAR-PCH as FBM method)

No added speckle noise		**Harris**	**FAST**	**Eigenvalues**	**SAR-PCH**
Before	Cross-correlation peak	199, 6			
	MSE	1.8465			
	PSNR	88.3482			
	Avgerage Coherence	0.8070			
ABM	Cross-correlation peak	0, 0			
	MSE	1.3164			
	PSNR	89.8177			
	Avgerage Coherence	0.8550			
FBM	No. of Matched Points	46	9	51	20
	Cross-correlation peak	0, 0	0, 0	0, 0	0, 0
	MSE	1.3159	1.3163	1.3161	1.3164
	PSNR	89.8154	89.8145	89.8130	89.8174
	Avgerage Coherence	0.8546	0.8546	0.8545	0.8546

Table 11. Experimental results of image pair No. 4, Using SAR-PCH directly as FBM method

No added speckle noise		**Harris**	**FAST**	**Eigenvalues**	**SAR-PCH**
Before	Cross-correlation peak	60, -40			
	MSE	2.3281e+4			
	PSNR	39.6223			
FBM	No. of Matched Points	4913	2694	4912	4448
	Cross-correlation peak	0, 0	0, 0	0, 0	0, 0
	MSE	801.0766	737.5834	802.9696	775.2573
	PSNR	53.8389	54.3471	53.8461	54.2118

Table 12. Experimental results of image pair No. 4, using the proposed approach (combination of ABM method and SAR-PCH as FBM method)

No added speckle noise		**Harris**	**FAST**	**Eigenvalues**	**SAR-PCH**
Before	Cross-correlation peak	60, -40			
	MSE	2.3281e+4			
	PSNR	39.6223			
ABM	Cross-correlation peak	0, 0			
	MSE	695.1755			
	PSNR	54.8715			
FBM	No. of Matched Points	4914	2696	4915	4447
	Cross-correlation peak	0, 0	0, 0	0, 0	0, 0
	MSE	797.6655	726.8659	790.4159	768.0225
	PSNR	53.8580	54.4108	53.9075	54.2517

Table 13. Experimental results of image pair No.4, using the proposed approach (combination of ABM method and SAR-PCH as FBM method)

Added a speckle noise with zero mean and different values of variances							
Variance of Speckle noise	***Similarity Metrices***	***Before***	***ABM***	***Harris***	***FAST***	***Eigen-values***	***SAP-PCH***
0.01	A	60,-40	0,0	0,0	0,0	0,0	0,0
	B	0.0801	0.0456	0.0455	0.0458	0.0456	0.0453
	C	10.9631	13.4121	13.4196	13.3881	13.4134	13.4384
0.05	A	60,-40	0,0	0,0	0,0	0,0	0,0
	B	0.1058	0.0597	0.0592	0.0598	0.0593	0.0590
	C	9.7555	12.2372	12.2735	12.2310	12.2690	12.2899
0.07	A	60,-40	0,0	0,0	0,0	0,0	0,0
	B	0.1192	0.0665	0.0658	0.0665	0.0662	0.0642
	C	9.2381	11.7691	11.8164	11.7730	11.7886	11.8243
0.09	A	60,-40	0,0	0,0	0,0	0,0	0,0
	B	0.1325	0.0731	0.0727	0.0734	0.0728	0.0709
	C	8.778	11.3602	11.3833	11.3440	11.3781	11.3967
0.1	A	60,-40	0,0	0,0	0,0	0,0	0,0
	B	0.1390	0.0763	0.0758	0.07694	0.0761	0.0739
	C	8.5690	11.1737	11.2029	11.1694	11.1844	11.2251

A ---- Location of Cross-correlation Peak
B ---- Mean Square Error (MSE)
C ---- Peak Signal-to-Noise Ratio (PSNR)

Table 14. Experimental results of image pair No.4,
Using SAR-PCH directly as FBM methods

Added a speckle noise with zero mean and different values of variances							
Variance of Speckle noise	***Similarity Metrices***	***Before***	***ABM***	***Harris***	***FAST***	***Eigen-values***	***SAP-PCH***
0.01	A	60,-40	-	0,0	0,0	0,0	0,0
	B	0.0801	-	0.0456	0.0458	0.0456	0.0453
	C	10.9626	-	13.4116	13.3949	13.4092	13.4427
0.05	A	60,-40	-	0,0	0,0	0,0	0,0
	B	0.1059	-	0.0592	0.0598	0.0591	0.0589
	C	9.7527	-	12.2759	12.2345	12.2811	12.3002
0.07	A	60,-40	-	0,0	0,0	0,0	0,0
	B	0.1191	-	0.0660	0.0665	0.0661	0.0659
	C	9.2412	-	11.8025	11.7699	11.7996	11.8113
0.09	A	60,-40	-	0,0	0,0	0,0	0,0
	B	0.1324		0.0727	0.0731	0.0730	0.0726
	C	8.7800	-	11.3836	11.3601	11.3678	11.3836
0.1	A	60,-40	-	0,0	0,0	0,0	0,0
	B	0.01391	-	0.0760	0.0765	0.0763	0.0755
	C	8.5652	-	11.1930	11.1633	11.1773	11.2179

A ---- Location of Cross-correlation Peak
B ---- Mean Square Error (MSE)
C ---- Peak Signal-to-Noise Ratio (PSNR)

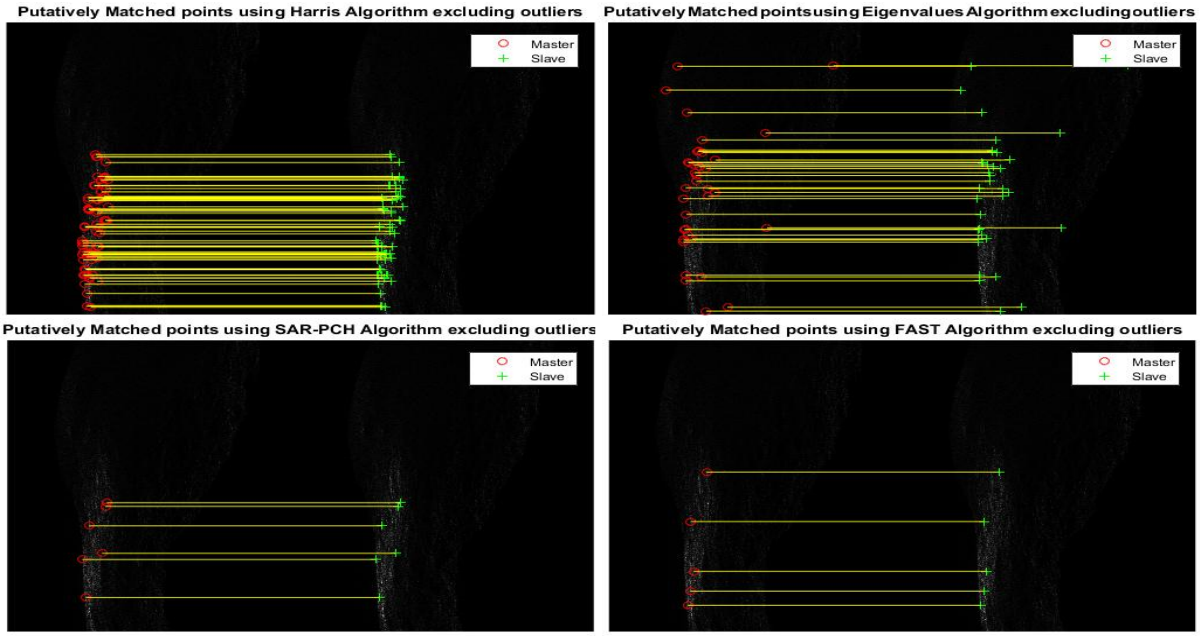

Fig. 12. Putatively matched points between images concerning pair no. 1

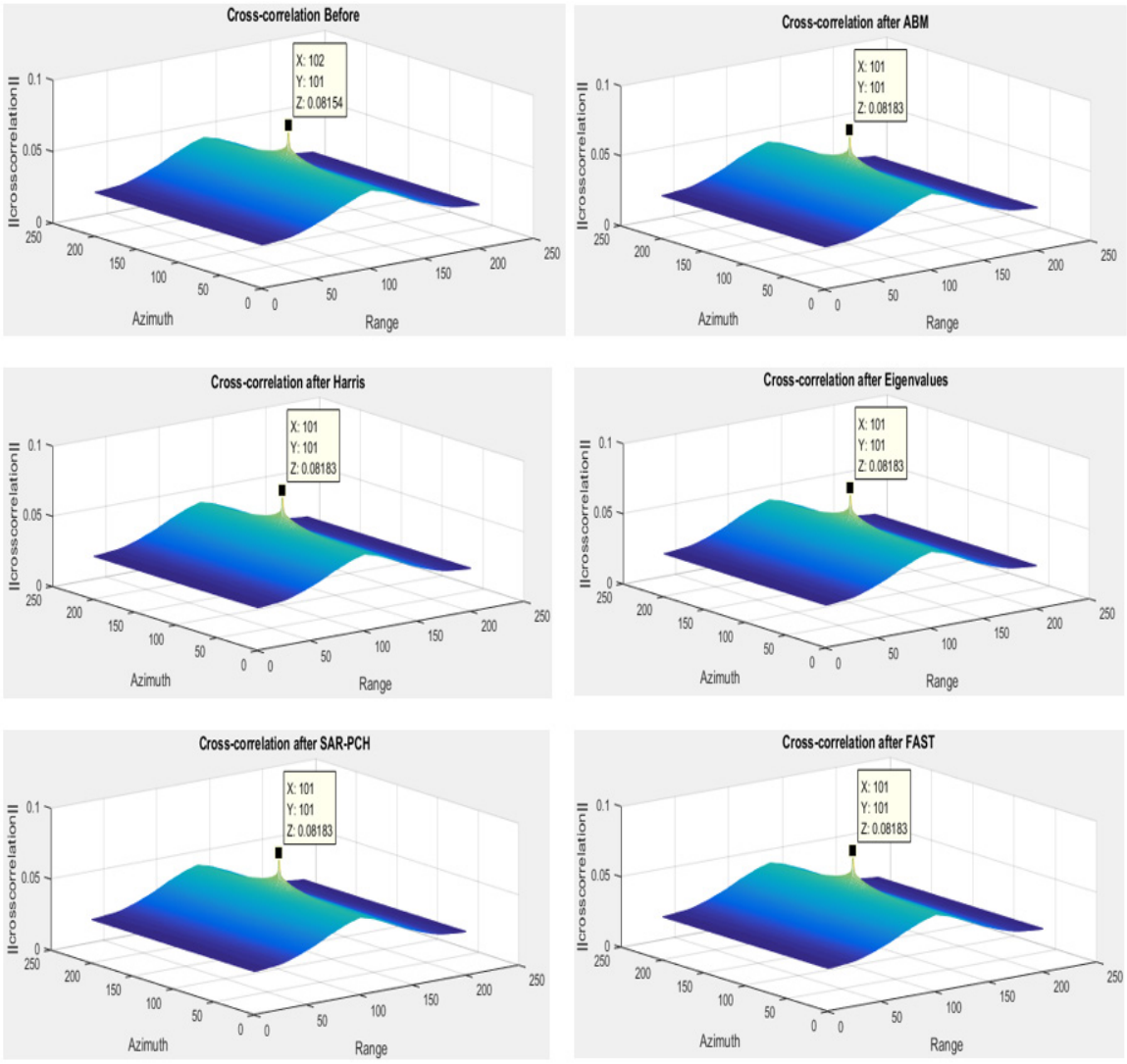

Fig. 13. Cross-correlation peak position concerning pair no. 1

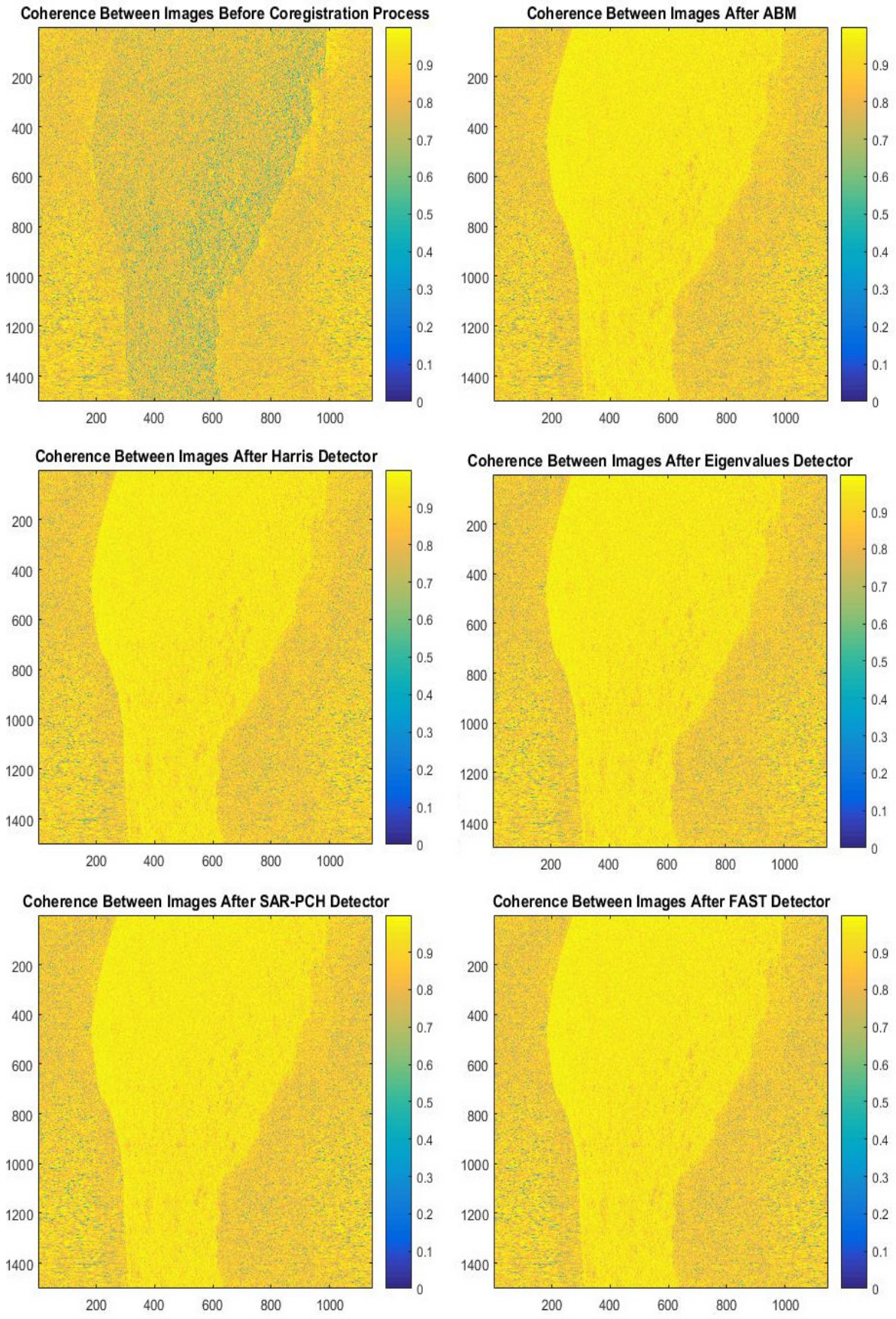

Fig. 14. Coherence map concerning pair no. 1

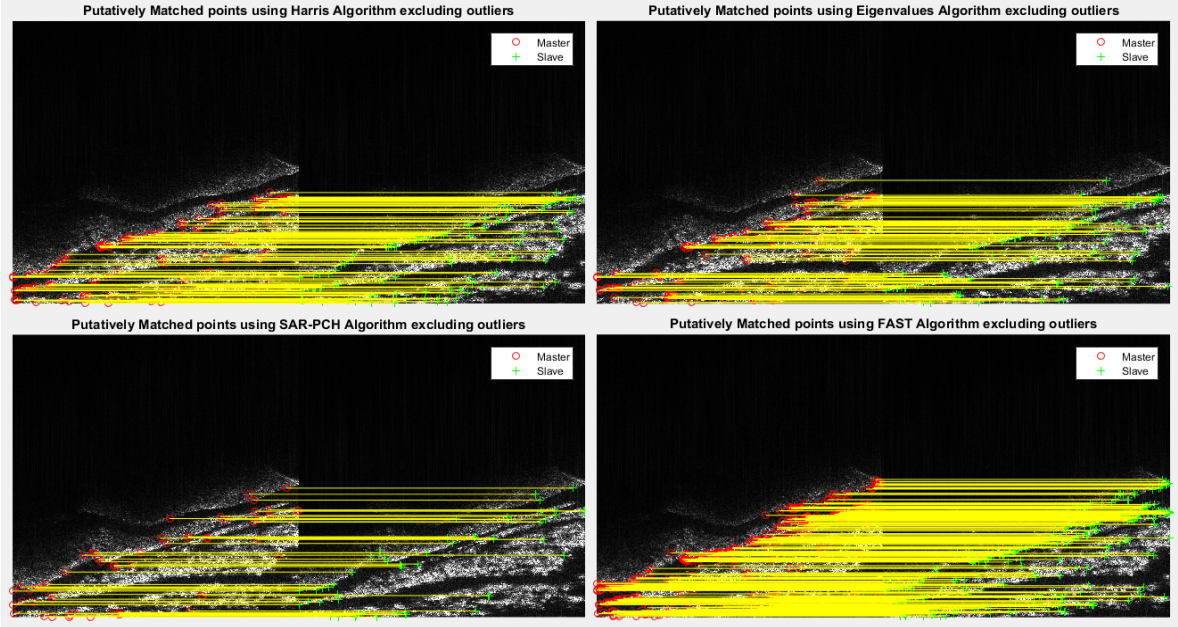

Fig. 15. Putatively matched points between images concerning pair no. 2

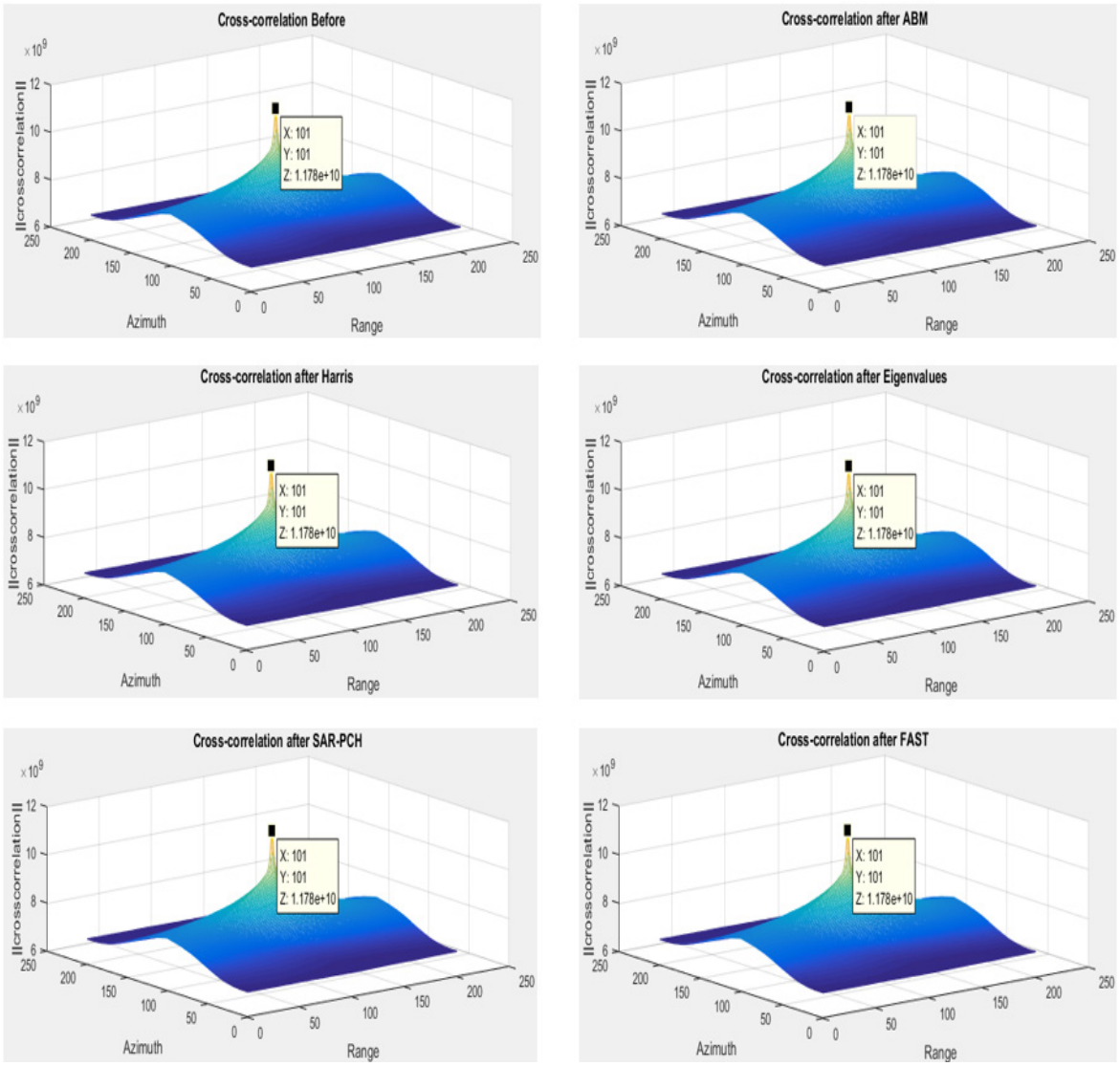

Fig. 16. Cross-correlation peak position concerning pair no. 2

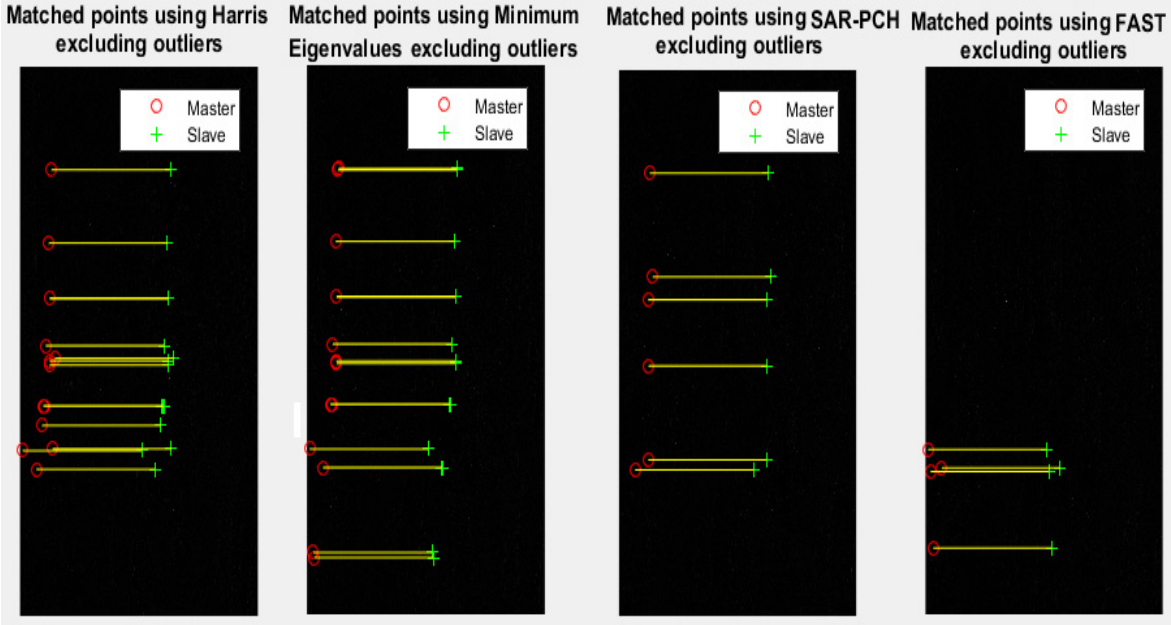

Fig. 17. Putatively matched points between images concerning pair no. 3

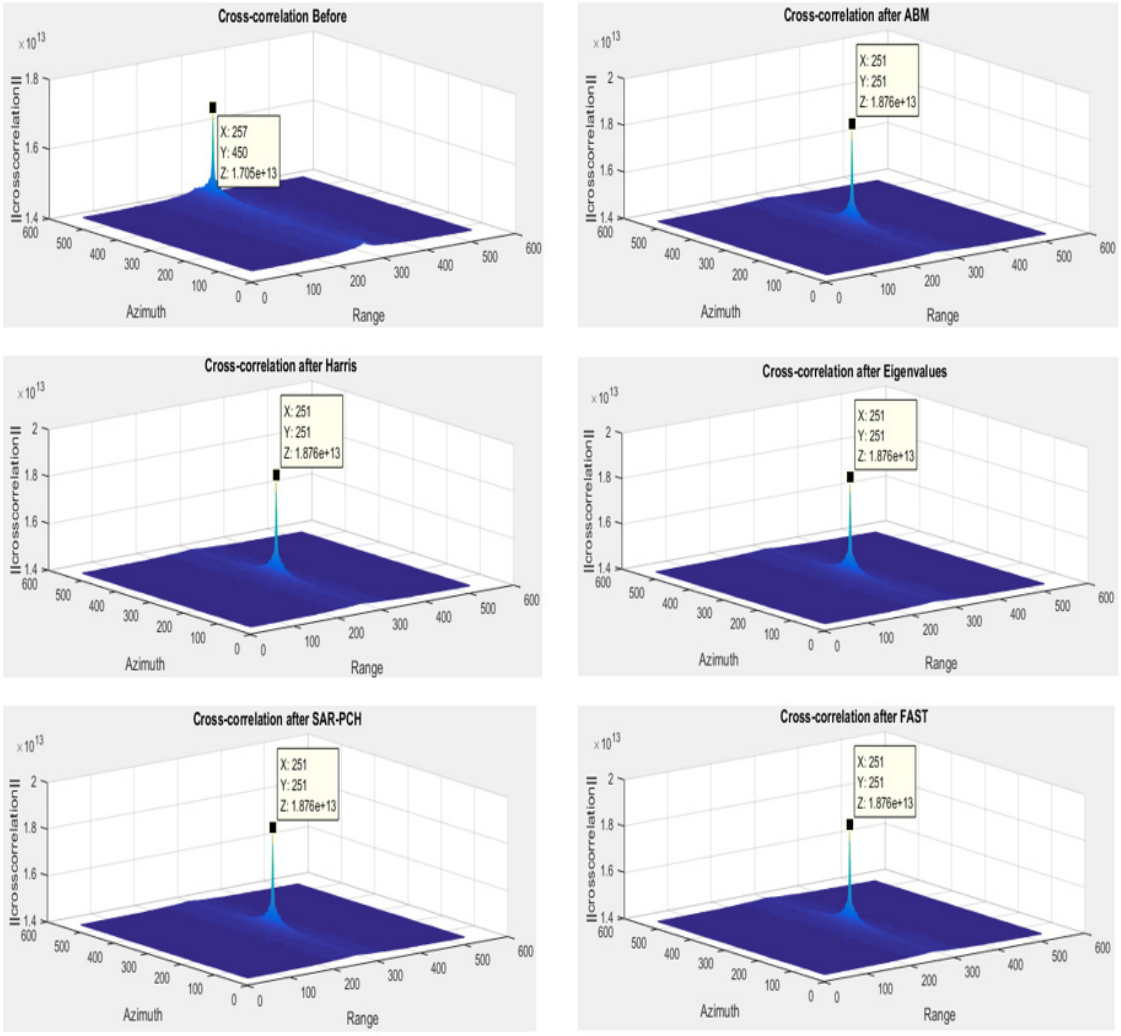

Fig. 18. Cross-correlation peak position concerning pair no. 3

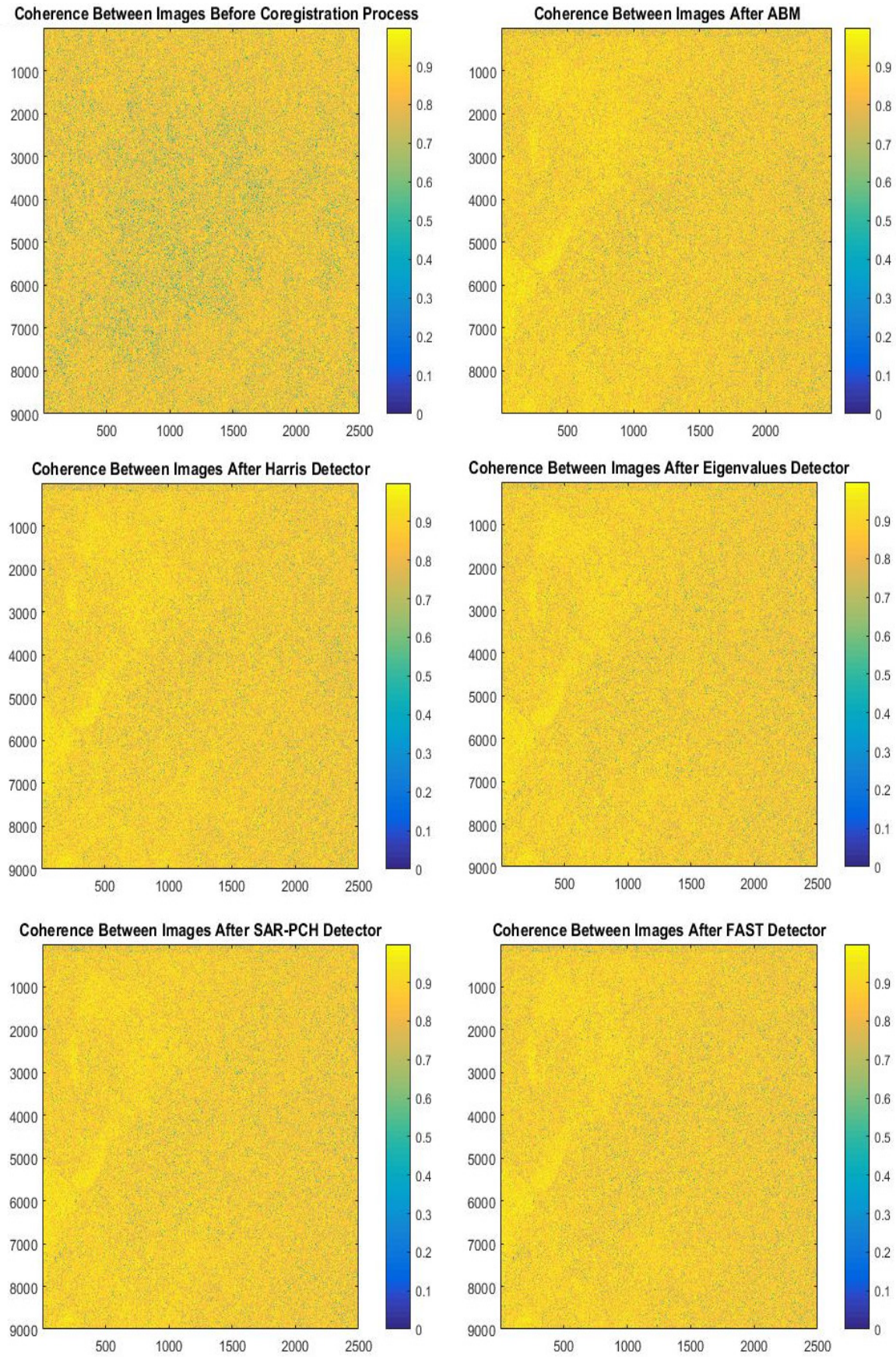

Fig. 19. Coherence map concerning pair no. 3

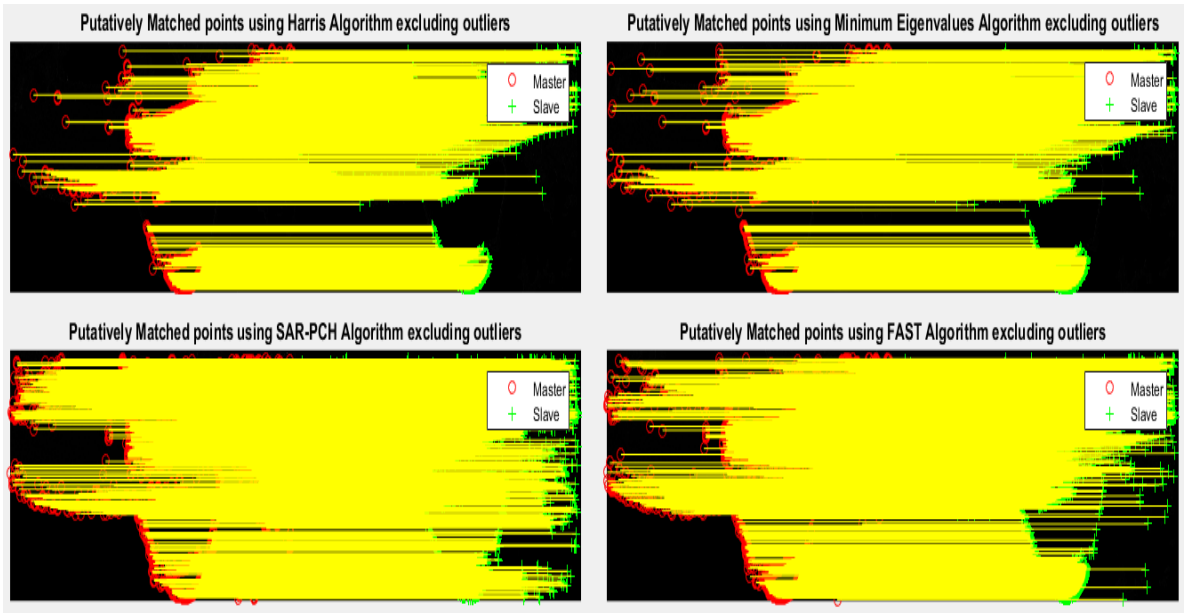

Fig. 20. Putatively matched points between images concerning pair no. 4

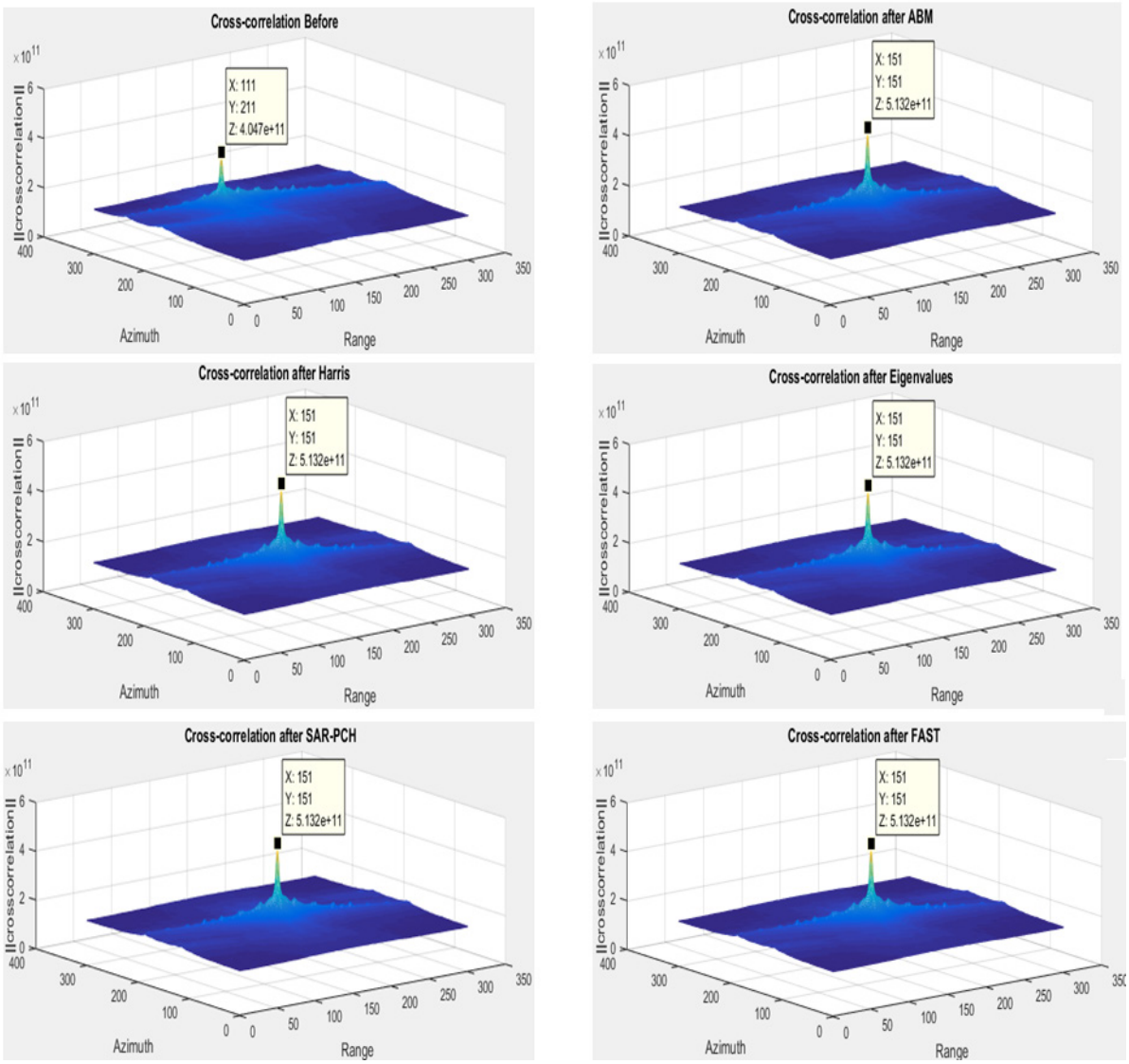

Fig. 21. Cross-correlation peak position concerning pair no. 4

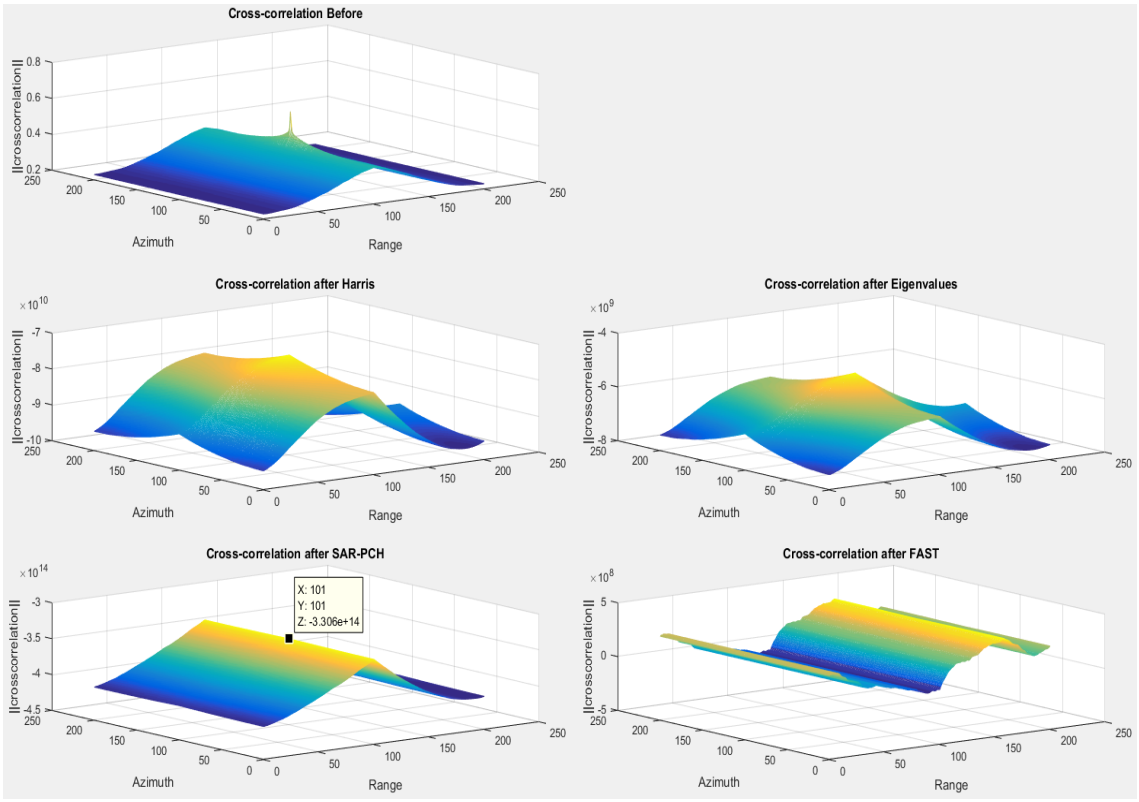

Fig. 22. Cross-correlation peak position concerning pair no. 1 without ABM with Noise var= 0.01

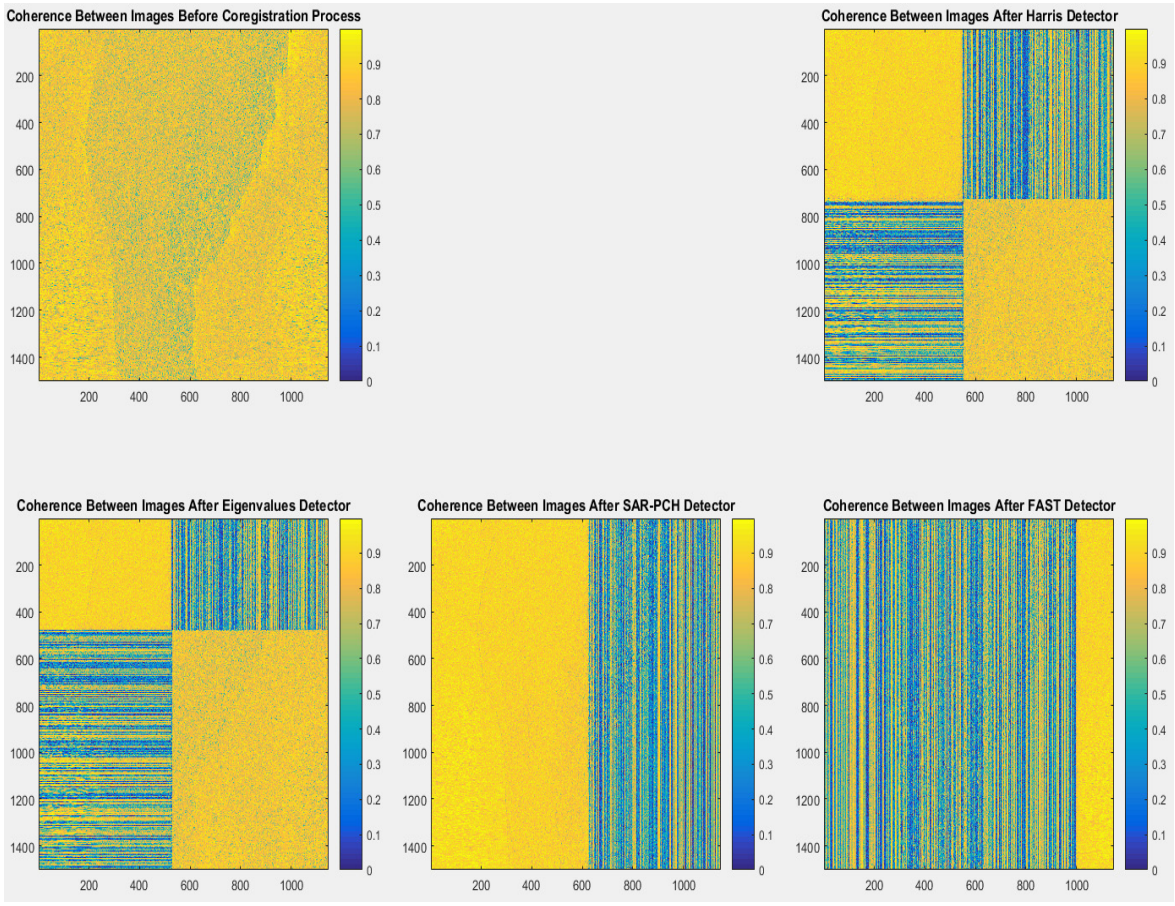

Fig. 23. Coherence of pair no. 1 without ABM with Noise var= 0.01

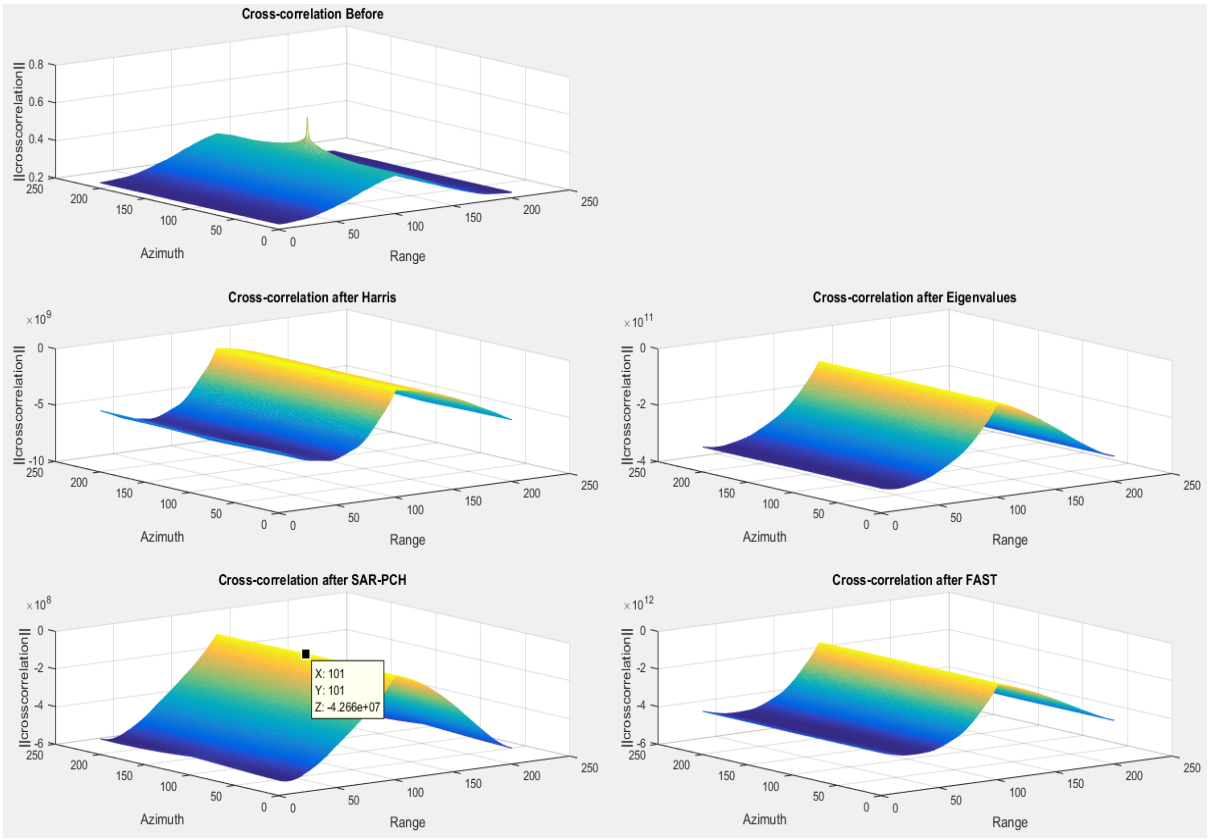

Fig. 24. Cross-correlation peak position concerning pair no. 1 without ABM with Noise var= 0.1

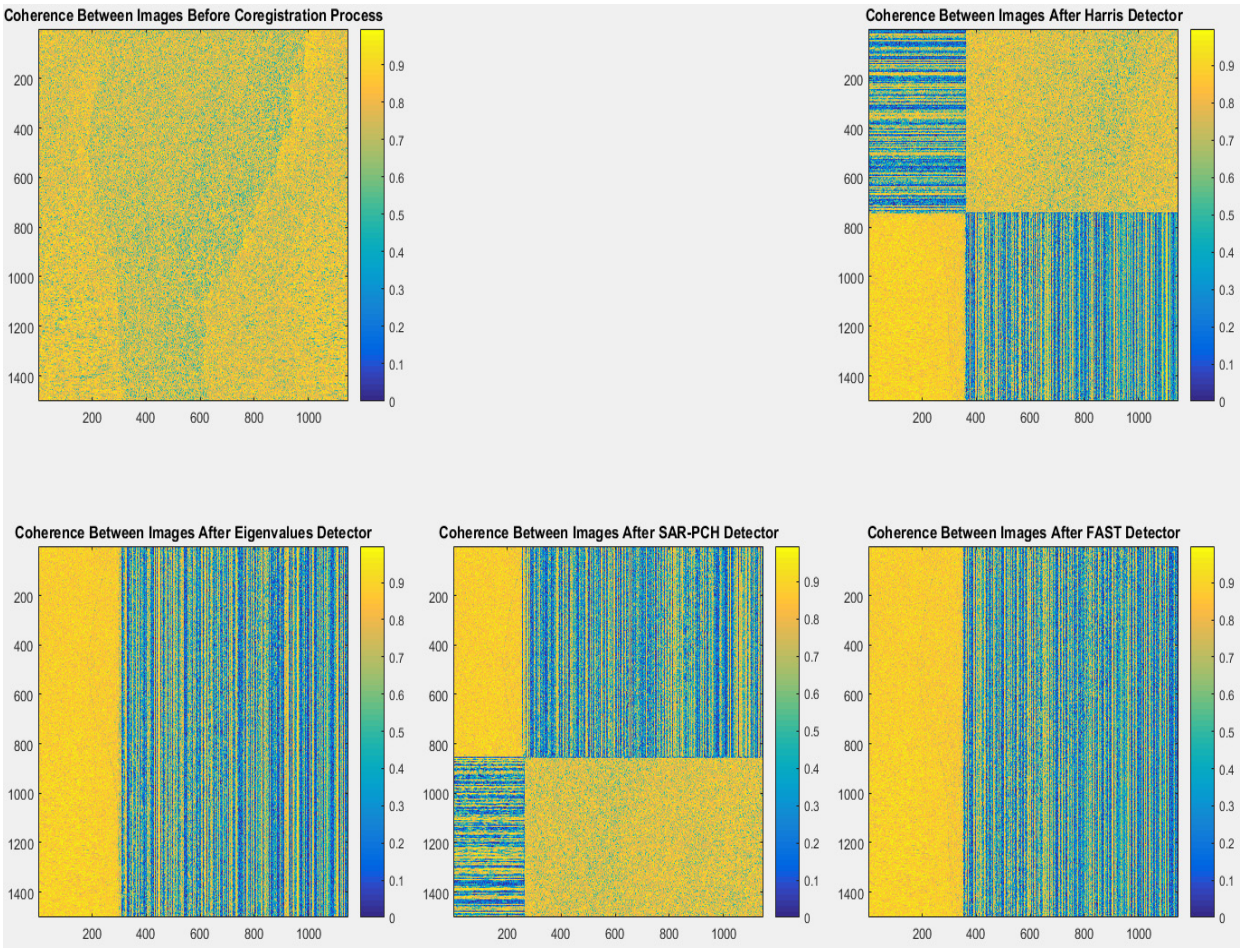

Fig. 25. Coherence of pair no. 1 without ABM with Noise var= 0.1

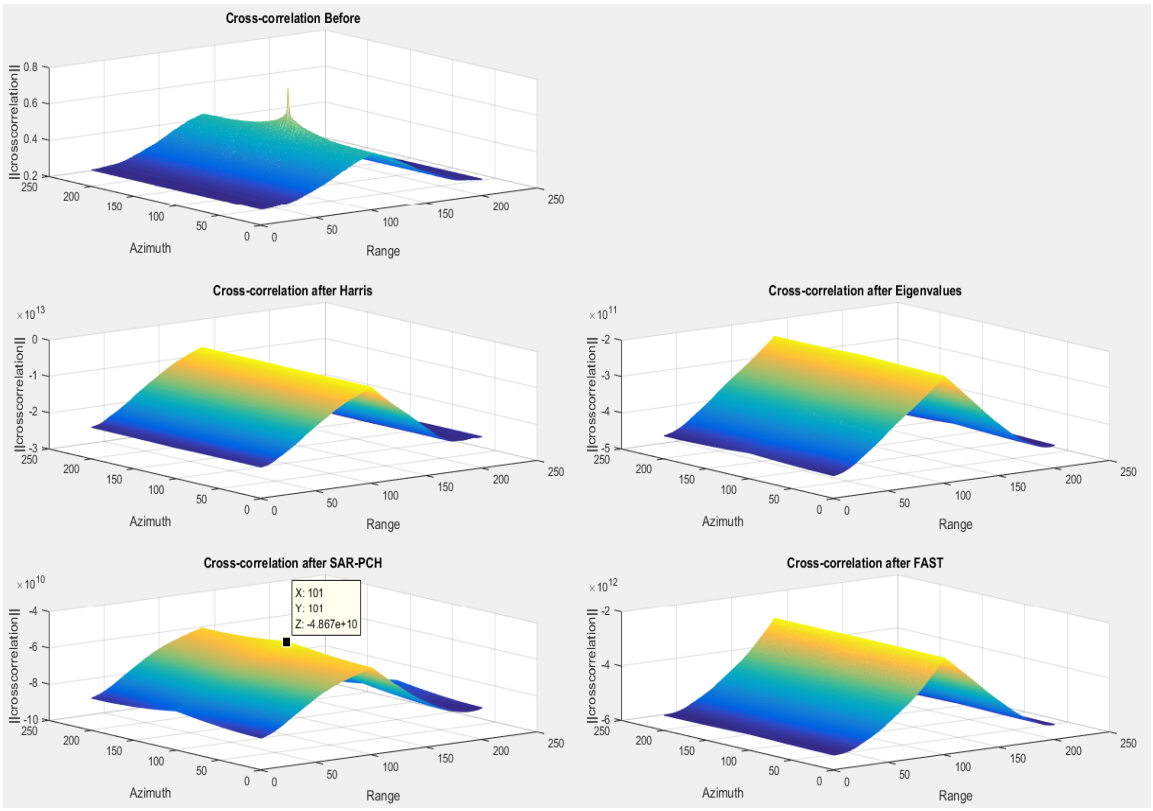

Fig. 26. Cross-correlation peak position concerning pair no. 1 without ABM with Noise var= 0.9

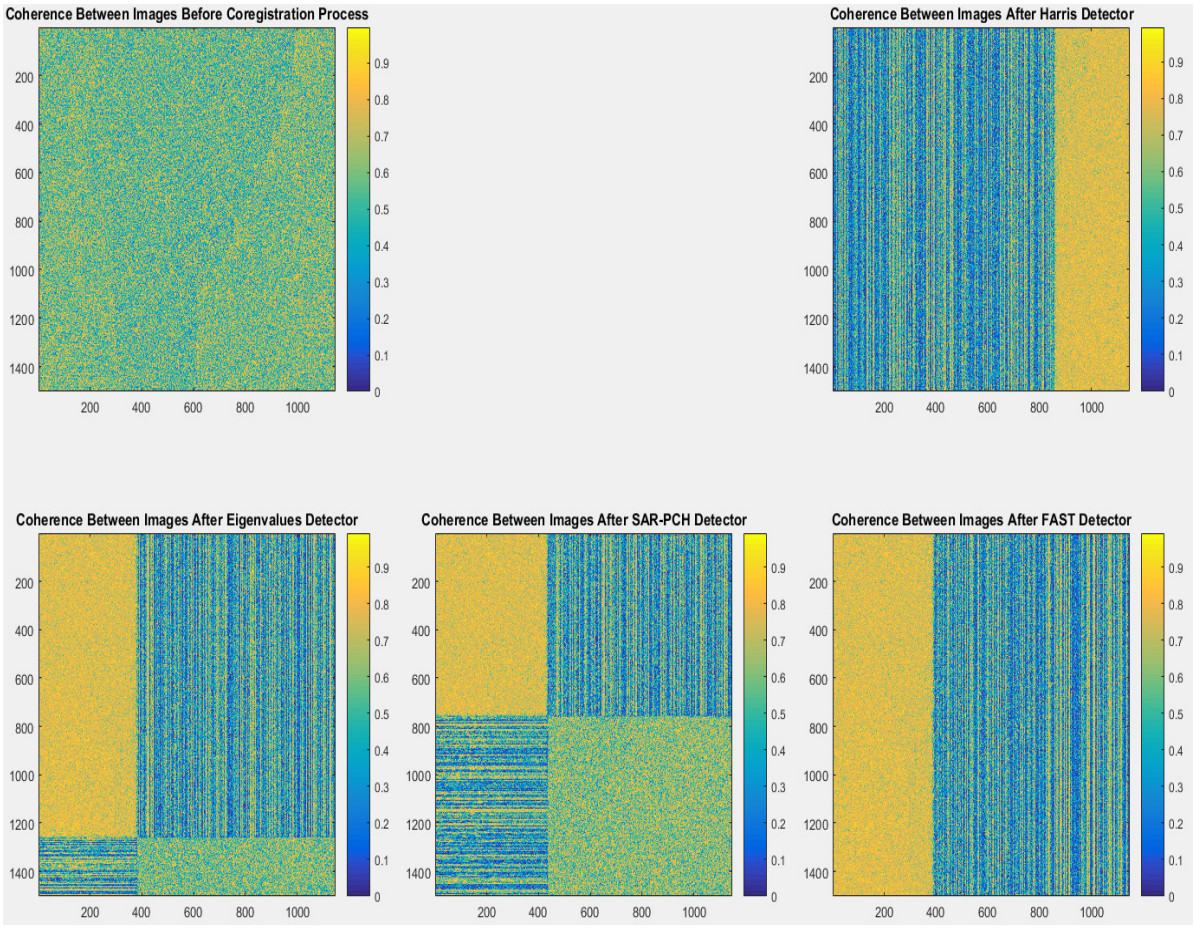

Fig. 27. Coherence of pair no. 1 without ABM with Noise var= 0.9

6. Conclusion

A modified corner detector named SAR-PCH (Synthetic Aperture Radar- Phase Congruency Harris) is proposed. It is based on a combination between both phase congruency algorithm and Harris corner detector where Phase Congruency (PC) image can supply fundamental and significative features although the complex changes of intensities and noise. The performance was compared with Shi-Tomasi, FAST, and Harris corner detectors. Experiments are conducted first with simulated images and second with real ones. The used dataset of SAR images were the only available ones. Of the evaluation steps, a speckle noise with zero mean and different values of variances are applied. That is to verify the effectiveness of the proposed algorithm where it overcomes the Harris corner limitation considering the noise. The shift between the input images (cross-correlation peak position), mean square error (MSE), peak signal-to-noise ratio (PSNR), and coherence factor are used as a similarity metrices for the simile to evaluate the performance.

The overall registration process is performed off-line. Experimental results are carried out in a standard computer and verifies the effectiveness of the proposed approach. The privileges of image constitutional depicting allow to detect and extract the most powerful keypoints since it preserves robustness of co-registration process where the frequency properties of the image are not variant to illumination or noise changes. Reasonable results were achieved compared to the state of art methods, on the expense of high computational cost and process time which can be recovered using hardware having higher capabilities. SAR-PCH corner detector is a highly localized tool for feature detection and has the privilege of being not sensitive to intensities and noise changes and hence overcomes the Harris limitations. Future work, it is planned to apply the proposed algorithm to further dataset having more complex scenes such as urban areas.

References

[1] Mahmoud Hassaballah, Khalid M. Hosny, Recent Advances in Computer Vision Theories and Applications, © Springer Nature Switzerland, vol. 804, 2019.

[2] Ertugrul Bayraktar, Pinar Boyraz, Analysis of feature detector and descriptor combinations with a localization experiment for various performance metrics, Turkish Journal of Electrical Engineering & Computer Sciences, 25 (2017) 2444-2454.

[3] Aboul Ella Hassanien, Mohamed F. Tolba, Khaled Shaalan, Ahmad Taher Azar, Advances in Intelligent Systems and Computing, Proceedings of the International Conference on Advanced Intelligent Systems and Informatics, © Springer Nature Switzerland, 845 (2019).

[4] Reshmi Krishnan, Anil. A. R., A Survey on Image Matching Methods, International Journal of Latest Research in Engineering and Technology (IJLRET) 2-1 (2016) 58-61.

[5] Niangang Jiao, Wenchao Kang, Yuming Xianga, Hongjian You, A Novel and Fast Corner Detection Method for SAR Imagery, International Archives of the Photogrammetry, Remote Sensing and Spatial Information Sciences XLII–2/W7 (2017).

[6] A.A. Karim, E. F. Nasser, Improvement of Corner Detection Algorithms (Harris, FAST and SUSAN) Based on Reduction of Features Space and Complexity Time, Engineering & Technology Journal, 35-B2 (2017).

[7] Ehab Salahat, Murad Qasaimeh, Recent Advances in Features Extraction and Description Algorithms: A Comprehensive Survey, arXiv:1703.06376, 1 (2017).

[8] M. Hassaballah and Ali Ismail Awad, Image Feature Detectors and Descriptors: Foundations and Applications, in: Ali Ismail Awad, Mahmoud Hassaballah (Eds.), Studies in Computational Intelligence, © Springer, Switzerland, 2016, pp. 11-47.

[9] Arthur Ardeshir Goshtasby, Theory and Applications of Image Registration, first ed., JohnWiley & Sons, Inc, 2017.

[10] Abdelhameed S. Eltanany, M. S. Elwan, and A. S. Amein, Key Point Detection Techniques, in: Aboul Ella Hassanien, Khaled Shaalan, Mohamed Fahmy Tolba (Eds.), Proceedings of the International Conference on Advanced Intelligent Systems and Informatics, Springer Nature, Switzerland, 2020, pp. 901-911.

[11] E.R. Davies, Computer Vision Principles, Algorithms Applications, Learning, fifth ed., Elsevier Inc., 2018.

[12] K Y Kok and P Rajendran, Validation of Harris Detector and Eigen Features Detector, International Conference on Aerospace and Mechanical Engineering (AeroMech17), 370 (2018).

[13] Wenping Ma, Yue Wu, Shaodi Liu, Qingxiu Su, and Yong Zhong, Remote Sensing Image Registration Based on Phase Congruency Feature Detection and Spatial Constraint Matching, IEEE Access 6 (2018) 77554-77567

[14] Zaafouri Ahmed, Mounir Sayadi and Farhat Faniech, Satellite Images features Extraction using Phase Congruency model, International Journal of Computer Science and Network Security (IJCSNS) 9-2 (2009) 192-197.

[15] Jyoti Malik, G. Sainarayanan and Ratna Dahiya, Corner Detection Using Phase Congruency Features, International Conference on Signal and Image Processing (2010) 217-221.

[16] Qiang Zhang, Yabin Wang, Long Wang, Registration of images with affine geometric distortion based on maximally stable extremal regions and phase congruency, Image and Vision Computing, (2015).

[17] A.F. Cinar, S.M. Barhli, D. Hollis, M. Flansbjer, R.A. Tomlinson, T.J. Marrow, M. Mostafavi, An autonomous surface discontinuity detection and quantification method by digital image correlation and phase congruency, Optics and Laser Engineering, 96 (2017) 94–106.

[18] Clive Trenton, Andrew Lambert, Detecting Space Debris using Phase Congruency, Engineering Project Report, University of New South Wales (UNSW)at Australian Defense Force Academy (DFA) (2017).

[19] Yuming Xiang, Feng Wang, Ling Wan and Y. Hongjian, SAR-PC: Edge Detection in SAR Images via an Advanced Phase Congruency Model, Remote Sensing-Open Access Journal (MDPI) 9-209 (2017) 1-28.

[20] Yuanxin Ye, Jie Shan, Siyuan Hao, Lorenzo Bruzzone, and Yao Qin, A local phase based invariant feature for remote sensing image matching, Journal of Photogrammetry and Remote Sensing (ISPRS) 142 (2018) 205-221.

[21] Mabuza-Hocquet G and Nelwamondo F, Fusion of Phase Congruency and Harris Algorithm for Extraction of Iris Corner Points, Third International Conference on Artificial Intelligence, Modelling and Simulation (2015) 315-320.

[22] Peter Kovesi, Image Features from Phase Congruency, Technical report 95/4, Department of Computer Science, The University of Western Australia (1995).

[23] Peter Kovesi, Image Features from Phase Congruency, Journal of Computer Vision Research, 1:3 (1999) 1-27.

[24] Peter Kovesi, Phase congruency: A low-level image invariant, Psychological Research, 64 (2000) 136-148.

[25] Peter Kovesi, Phase Congruency Detects Corners and Edges, in: Sun C., Talbot H., Ourselin S. and Adriaansen T. (Eds.), Proc. VIIth Digital Image Computing: Techniques and Applications, Sydney, 2003, pp. 309-318.

[26] Zheng Liu and Robert Laganiere, On the Use of Phase Congruency to Evaluate Image Similarity, IEEE International Conference on Acoustics Speech and Signal Processing Proceedings, II (2006) 937-940.

[27] Adrian Burlacu and Corneliu Lazer, Image Features Detection using Phase Congruency and Its Application in Visual Servoing, Fourth International Conference on Intelligent Computer Communication and Processing (2008) 47-51.

[28] Y. L. Malathi Latha, Local Feature Integration Method Using Phase Congruency for Palm Print Authentication, International Journal of Image and Graphics 15:3 (2015) 1550008(1-17).

[29] H.D. Supreetha Gowda and G. Hemantha Kumar, Evaluation of Texture Features for Biometric Verification System Using Handvein and Finger Knuckle print, in: K.C. Santosh, Mallikarjun Hangarge, Vitoantonio Bevilacqua, Atul Negi (Eds.), Communications in Computer and Information Science 709, Springer Nature Singapore Pte Ltd., 2017, pp. 420-428.

[30] Zhen Ye, Xiaohua Tong, Illumination-Robust Subpixel Fourier-Based Image Correlation Methods Based on Phase Congruency, IEEE Transaction on Geoscience and Remote Sensing (2018).

[31] C. Harris and M. Stephens, A combined corner and edge detector, Alvey Vision Conference (1988) 147-151.

[32] Moravec, H.P., Towards automatic visual obstacle avoidance, Fifth International Joint Conference on Artificial Intelligence (1977) 584-594.

[33] Shi, J., and C. Tomasi., Good Features to Track, IEEE Conference on Computer Vision and Pattern Recognition (CVPR94) Seattle (1994)

[34] Joanna Janicka, Jacek Rapinski, Outliers Detection by RANSAC Algorithm in the Transformation Of 2D Coordinate Frames, Geodetic Sciences Bulletin Online version, 20:3 (2014) 610-625.

[35] Rosten, E., Drummond, T., Machine learning for high speed corner detection, in: A. Leonardis, H. Bischof, and A. Pinz (Eds.), Ninth European Conference on Computer Vision I, Springer-Verlag Berlin Heidelberg, 2006, pp. 430-443.

[36] Förstner, W; Gülch, A Fast Operator for Detection and Precise Location of Distinct Points, Corners and Centers of Circular Features, International Society for Photogrammetry and Remote Sensing ISPRS, inter-commission workshop, 1987.